

# Transport of ions in solution and across membranes

- 7-1. Introduction
- 7-2. Ionic fluxes in solutions
  - 7-2.1. Fluxes due to an *electrical field* in a solution
  - 7-2.2. Flux due to an *electrochemical potential gradient*
- 7-3. Transmembrane potentials
  - 7-3.1. The Nernst potential, the single ion case where the flux is zero
  - 7-3.2. Current-voltage relationships of ionic channels
  - 7-3.3. The constant field approximation
  - 7-3.4. The case of a neutral particle
- 7-4. The resting transmembrane potential, *ER*
  - 7-4.1. Goldman-Hodgkin-Katz expression for the resting potential
  - 7-4.2. Gibbs-Donnan equilibrium and the Donnan potential
  - 7-4.3. Electrodifusion
- 7-5. Patch clamp studies of single-channel kinetics
- 7-6. The action potential in excitable cells
  - 7-6.1. Neuronal currents
  - 7-6.2. The Hodgkin-Huxley nerve action potential
  - 7-6.3. The voltage clamp methods for measuring transmembrane currents
  - 7-6.4. Functional behavior of the nerve axon action potential
  - 7-6.5. Cardiac and other action potentials
- 7-7. Propagation of the action potential
  - 7-7.1. The cable equations
  - 7-7.2. The velocity of propagation
- 7-8. Maintaining ionic balance: Pumps and exchangers
- 7-9. Volume changes with ionic fluxes
- 7-10. Summary
- 7-11. Further reading
- 7-12. Problems
- 7-13. References
  - 7-13.1. References from previous reference list not appearing in current text or references

[This chapter lacks the following: Tables and programs. Completion of later parts on the pumps. Complete cross referencing. Improvements in Figures.](#)

## 7-1. Introduction

The transport of ions across cell membranes is essential to life. Most of it is passive, due to electrical and chemical concentration differences. The electrochemical potential difference is the key to excitation of the cells, for it governs the opening and closing of channels and drives ionic flows and therefore governs the transmembrane potential. Ionic channels are remarkably

ion-selective, the conductivity for a particular ion being substantially higher than for even rather similar ions, and ionic flux is passive, driven by the ion's electrochemical gradient. Ionic pumps, powered by ATP or by energy gradients for other solutes, are needed to restore the balance.

Cellular excitation drives many processes, the most obvious being contraction of muscle cells and signalling. The spatial propagation of a wave of depolarization along nerves or along a muscle cell is a highly efficient means of signal transmission over long distances without substantial mass transfer. Electrical conductivity of tissues and of membranes plays a role in regulation of other functions of cells: just as depolarization of a nerve axon leads to a conducted action potential, and depolarization of skeletal muscle, smooth muscle, and cardiac cells leads to activation of contraction, the depolarization of the pancreatic beta cell is associated with the release of insulin.

In nerve cell bodies and in axons the spikes of depolarization are short, one or two milliseconds. The local depolarizations are propagated along axons or dendrites to carry information; the neuronal cell bodies serve as integrators of trains of propagated spike depolarizations from a few or many dendrites and, in turn, if stimulated past a threshold level, send out spikes of depolarization along a major axon. Each propagated action potential, each depolarization spike, is due to the passage of a few thousand ions across the membrane, a molar amount that is so small as to be negligible compared to the ambient concentrations on either side of the membrane. Yet, to maintain the tissue in steady state, each ion must be moved back across the membrane, with the expenditure of energy from the hydrolysis of ATP directly or indirectly. Some ions are pumped back using direct coupling to ATP as the energy source. For example, the NaK ATPase pumps 3 Na<sup>+</sup> out and 2 K<sup>+</sup> inward for each ATP degraded to ADP. Other transporters use the energy from standing gradients, for example, the NaCa exchanger (NaCaX) extrudes 1 Ca<sup>++</sup> for 3 Na<sup>+</sup> flowing inward down the electrochemical gradient for Na<sup>+</sup>.

The ionic concentration differences, coupled with the Donnan effect due to the high concentrations of negatively charged proteins within cells, result in cellular transmembrane potentials that are negative, defined as the inside potential being negative compared to the outside or extracellular potential. Thus, "resting" (meaning "unstimulated") cell membrane potentials are always negative, ranging from about -10 mV for the erythrocyte to -80 to -90 mV for excitable muscle cells and neurons.

Starting from the concepts of Chapter 4, concerning "Ions in Solution" and their behavior in an electrical field, this chapter covers transmembrane potentials due to single and multiple ionic gradients, the resting membrane potential, action potentials, electrical propagation at the cell level, and the gradient-restoring pumps and exchangers.

## 7-2. Ionic fluxes in solutions

### 7-2.1. Fluxes due to an *electrical field* in a solution

The flux of an ion due to a gradient in an electrical field follows the same Ohm's law type relationships that pertain for other transport processes, given that the concentrations are small enough, that the activity coefficients are constant and close to unity, and the system is linear. The velocity of each ion depends on the strength of the field,  $d\Psi/dx$ , and its mobility,  $u$ , which is inversely proportional to the frictional resistance between the molecule and the solvent,  $f_s$ , while the total flux depends also on the number of mobile ions, the concentration,  $C$ :

$$J_e = L_e X_e = -L_e \cdot \frac{\Delta\Psi}{\Delta x}, \quad (7-1)$$

$$J_e = -Cu \frac{\Delta\Psi}{\Delta x} = -C \left( \frac{zF}{f_s \mathfrak{N}_A} \right) \frac{\Delta\Psi}{\Delta x}, \quad (7-2)$$

where  $J_e$  = flux per unit cross-sectional area due to electric field, moles  $\text{s}^{-1} \text{cm}^{-2}$ ,  $L_e$  = electrical conductance, mhos,  $X_e$  = local electrical force or field strength, volts/cm;  $\Psi$  = potential, volts;  $u$  = mobility = velocity of the ion per unit potential gradient,  $\text{cm s}^{-1}$ ;  $C$  = concentration, molar;  $z$  = valence;  $F$  = Faraday, 96,485 coulombs/mole;  $\mathfrak{N}_A$  = Avogadro's number,  $6.0221 \times 10^{23}$  molecules  $\text{mol}^{-1}$ ;  $f_s$  = frictional resistance,  $\text{g} \cdot \text{cm}$ . This latter expression, the rightmost part of Eq. 7-2, reveals that the mobility is now described by  $zF/(f_s \mathfrak{N}_A)$ , the reciprocal of the frictional resistance divided by the charge per unit molecule (the charge,  $zF$ , divided by Avogadro's number,  $\mathfrak{N}_A$ ), thus identifying the Einstein relationship,  $D = uRT/|z|F$ , or  $D = \mathfrak{R}T/f_s \mathfrak{N}_A$ ,  $\text{cm}^2/\text{s}$ .

### 7-2.2. Flux due to an *electrochemical potential gradient*

Flux produced by an *electrochemical* gradient combines the fluxes due to the electrical and chemical potential gradients:

$$J_s = -\frac{C\mathfrak{R}T}{f_s \mathfrak{N}_A} \left( \frac{d \ln C}{dx} + \frac{zF}{\mathfrak{R}T} \frac{d\Psi}{dx} \right); \quad (7-3)$$

where  $f_s$  is the frictional coefficient (described in Chapters 4 and 5); the activity coefficient (not shown) is assumed to be unity, so ionic activity = concentration  $C$ ; the conductance per ion,  $L_e = \mathfrak{R}T/f_s \mathfrak{N}_A$ ; and  $J_s$  is the net flux per unit area through a conducting solution, or within a channel in a membrane, or in slits between endothelial cells. Using the definition of the diffusion coefficient  $D = \mathfrak{R}T/f_s \mathfrak{N}_A$ , this is seen to be the Nernst-Planck equation:

$$J_s = -D \left( \frac{dC}{dx} + \frac{zFC}{\mathfrak{R}T} \frac{d\Psi}{dx} \right). \quad (7-4)$$

The result is a combination of Fick's first law for diffusion down a concentration gradient (a net flux expression where the flux is passive diffusion), with the effects of a directed force,  $d\Psi/dx$ , driving the ion down the electrical field; *down* means away from the position of highest potential of the same charge as the ion.

## 7-3. Transmembrane potentials

### 7-3.1. The Nernst potential, the single ion case where the flux is zero

Now consider cases where the "gradient" is an electrochemical *potential difference* across a membrane. (Due to the fact that one doesn't know exactly either the thickness of a lipid bilayer forming a cell membrane or the shape of the electrical field within the bilayer, the word "gradient" really describes a  $\Delta\Psi$  rather than a true gradient  $d\Psi/dx$ ).

First consider the situation in which there is membrane conductivity for only one ion, such as  $K^+$  with KCl on both sides of the membrane. When the transmembrane ionic flux through an open channel is zero, the electrolyte is in a steady state with respect to the electrochemical gradient, that is, the concentration and electrical driving forces are in balance. Hence the expression within the brackets in Eq. 7-3 must equal zero, since the conductance  $L$  is not zero; that is,

$$\frac{d \ln C}{dx} + \frac{zF}{\mathfrak{R}T} \frac{d\Psi}{dx} = 0 \quad (7-5)$$

$$\Psi_1 - \Psi_2 = \Delta\Psi = \frac{\mathfrak{R}T}{zF} \ln(C_2/C_1) = 2.303 \frac{\mathfrak{R}T}{zF} \log_{10}(C_2/C_1)$$

This is the Nernst equation. The 2.303 is  $\log_e(10)$ . It assumes equal activity coefficients on the two sides of the membrane. For univalent ions the slope,  $2.303RT/zF$ , of the potential-concentration relationship is about 60 mV per decade (10-fold) change in ionic concentration; for divalent ions it is 30 mV/decade. Values for  $RT/zF$  depend only on temperature: with  $R = 8.3145 \text{ J mol}^{-1} \text{ K}^{-1}$  (or  $1.987 \text{ cal mol}^{-1} \text{ K}^{-1}$ ) where K is degrees Kelvin and  $T(\text{K})$  is temperature in degrees Kelvin or  $273.16 + T$  (Celsius). Values of  $RT/zF$  are in Table 7-1.

**Table 7-1:  $RT/zF$  at various temperatures**

$T$ , deg C	$RT/zF$ , mV	$2.303$ $RT/zF$ , mV
0	23.54	54.2
20	25.26	58.17
30	26.12	60.15
37	26.73	61.54

Typical values of Nernst potentials at 37 C,  $E_x$  for sodium and other ions are in Table 7-2. With  $Na_o = 140 \text{ mM}$  and  $Na_i = 12 \text{ mM}$ , then  $E_{Na} = 61.54 \times \log_{10}(140/12) = +65.7 \text{ mV}$  in heart.

**Table 7-2: Nernst Potentials in Mammalian Cells at 37° C**

Cell type	Ion	$[Ion]_{out}$ mM	$[Ion]_{in}$ mM	$E_{ion}$ , mV	Reference
Cardiomyocyte, ventricle at 37C	Na	138	10	+70.1	Michaelova '01
	K	4	159.5	-98.5	Michaelova '01
	Ca	2	$2 \times 10^{-4}$	+125.1	Michaelova '01
Renal tubule epithelium. at 37 C	Na	140	35	+ 37	
	K	5	130	- 87.1	
	Ca	2	$1 \times 10^{-4}$	+132.3	

**Table 7-2: Nernst Potentials in Mammalian Cells at 37° C**

Cell type	Ion	[Ion] <sub>out</sub> mM	[Ion] <sub>in</sub> mM	$E_{ion}$ , mV	Reference
Squid Giant Axon	Na	460	49	+ 56.4	Hodgkin,1951
at 18.5 C	K	22	410	- 73.5	Hodgkin,1951
	Cl	540	40	- 65.4	Hodgkin,1951
Human Endothelial Cell	Na	140	20		
at	K	5			
	Ca	2	$1 \times 10^{-4}$		

### 7-3.2. Current-voltage relationships of ionic channels

A membrane has capacitance of about  $1 \mu\text{F}/\text{cm}^2$ , a consequence of the form of the phospholipid bilayer, two layers of hydrophilic terminal phosphate groups separated by a very thin layer of insulating fatty acid tails; the insulating part is effectively about 2.3 nm thick, given a dielectric constant of about 2.1 for hydrocarbon chains. (The membrane capacitance is difficult to measure accurately, so this value of  $1 \mu\text{F}/\text{cm}^2$  is used everywhere, for any cell membrane. However, Sachs (1994) has found that a better value for mammalian cardiac cell membranes is about  $0.6 \mu\text{F}/\text{cm}^2$ .)

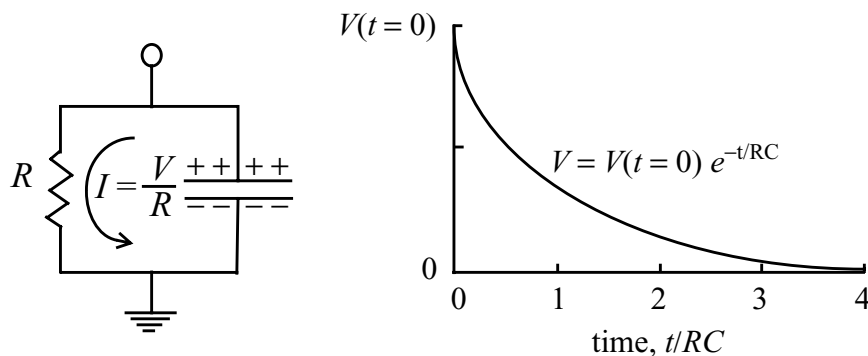


Figure 7-1: An RC circuit: a resistor  $R$  and a capacitor  $C$ , equivalent to a membrane. The discharge of a potential  $V$  across the membrane is a monoexponential process with time constant equal to  $RC$ .

An equivalent circuit for a pore through a membrane is shown in Fig. 7-1. The initial charge,  $Q$  coulombs, on the capacitor is  $V(t=0)$ , volts, times the capacitance  $C$ , farads. The rate of discharge  $dV/dt$  is the current, amperes or coulombs/second, divided by the capacitance, and, given that the current can only flow through the resistance, is given by Eq. 7-6, from Ohm's law:

$$\frac{dV}{dt} = -\frac{I}{C} = -\frac{V}{RC} \quad (7-6)$$

The solution of this ordinary differential equation,  $dV/dt = -V/RC$ , shows that the potential dissipates exponentially, given that  $R$  and  $C$  are constant:

$$V(t) = V(t=0)e^{-t/RC}, \quad (7-7)$$

in which form it is apparent that  $RC$  is the time constant for the exponential decay.

When there is a single ion carrying the current across the membrane with the driving force being a difference in the concentration of the ion on the two sides, the system acts like a battery, holding the voltage at the Nernst potential. Since there is no counter-ion flow, then when the ion-specific channel is opened a few thousand ions flow across, charging the membrane, and when the Nernst potential is reached the flow stops, but the battery remains charged. The diagram of Fig. 7-1 must then be revised, as shown in Fig. 7-2, and the diminution of charge of the capacitor is

$$\frac{d}{dt}VC = I = \frac{V - V_K}{R} = g_K(V - V_K), \quad (7-8)$$

where  $g_K$  is the conductance, in Siemens or  $\text{ohms}^{-1}$ , for potassium, and  $V_K$  is its Nernst potential from Eq. 7-5. A brief exercise is to show that  $RC$  has the units of time. Use the Terminology (Chapter 1) to provide conversion factors.

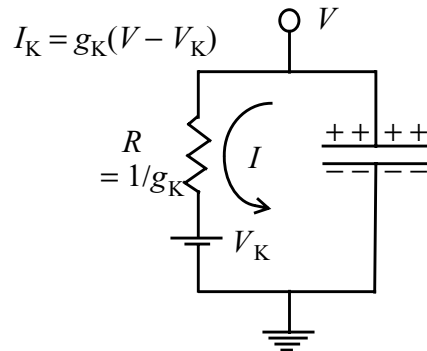


Figure 7-2: Equivalent circuit for a membrane current discharging while the potential is maintained by a battery. In the case of the only channel with non-zero conductance being potassium, the battery potential is the Nernst potential for  $\text{K}^+$ , which is maintained by the NaK pump, the NaK ATPase.

**Example Problem.** Four sets of situations are diagrammed in Fig. 7-3. The situations are the currents resulting from differing combinations of a passive leak conductance and a voltage-dependent conductance in parallel. Write a single program to reproduce all of the situations merely by changing the parameters. The circuit diagrams in the figure are equivalent to only the left branch of the circuit in Fig. 7-2, so you may assume that the current is in steady state. Determine the observed current as a sweep is made through a voltage range from  $-150$  mV to  $+150$  mV. Use a potassium conductance  $g_K$  of  $1 \text{ mS/cm}^2$ .

*Hint:* Make use of the Boltzmann relation for the fraction of open channels:

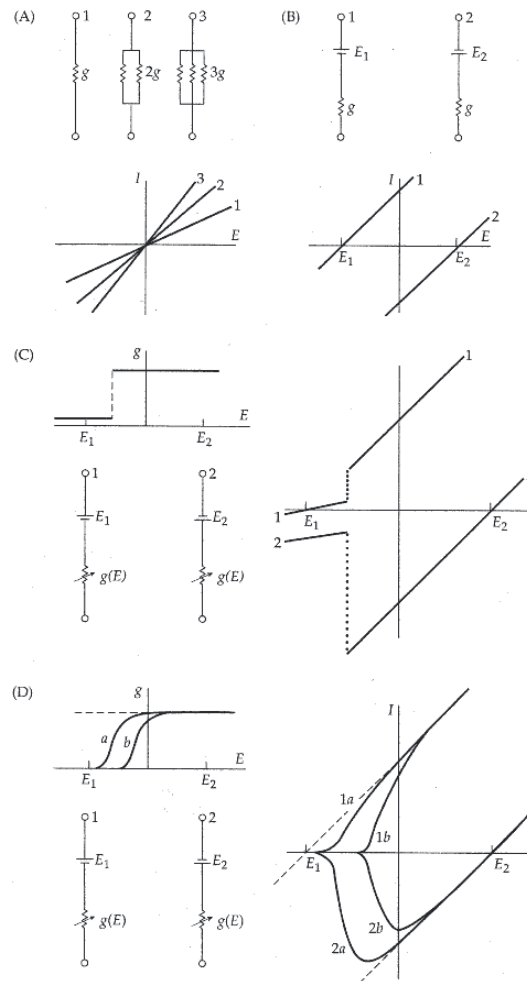


Figure 7-3: Current voltage relationships for a membrane with a single channel type, using Eq. 7-8. The voltage range from  $-100$  mV to  $+100$  mV covers the important biological range for most excitable cells. (Figure from Hille, 2001, Figure 1.6, page 19, with permission.)

$$\frac{\text{Open}}{\text{Open} + \text{Closed}} = \frac{1}{1 + e^{-z_g(q_e E)/(k_B T)}} = \frac{1}{1 + e^{-z_g q_e (E_m - E_{chan})/(k_B T)}}, \quad (7-9)$$

where  $E$  is a potential difference between the membrane potential,  $E_m$ , and the potential at which the channel is half open,  $E_{chan}$ ;  $z_g$  is the number of charges per channel protein that are moved across the membrane with a voltage jump;  $q_e$  is the elementary charge,  $k_B$  is the Boltzmann constant, and  $T$  is temperature, degrees Kelvin. Note that  $k_B T/q_e = RT/F$ .

**Answer to Problem.** The program describes a voltage-independent leak conductance and conductance via a voltage-dependent channel, without a capacitance. The solutions are not time-dependent, and require only algebraic equations. JSim code that can be used with different parameters for each of the I-V relationships in the Figure 7-3 is given in Table 7-3.

For A, choose values for the conductance  $g$  with ratios of 1:2:3.

For B, change the concentrations of potassium on the two sides.

**Table 7-3: Voltage-dependent currents for a leak and a channel**

```

JSim v1.1 //Vboltzmann.mod
// Program for potassium conductance versus voltage with gated channel
// Model for monovalent cation in water driven by electrochem gradient
// Membrane separates 2 regions of fixed concentrations, Ko and Ki
// Solute activities are unity. Currents reach S.S. instantaneously
// Single channel conductance about 300 pSiemens; 10^6 chan -> 300 uS.

import nsrunit; unit conversion on;
math Vboltzmann {realDomain Em mV; Em.min = -150; Em.max= 150; Em.delta=1;
//PARAMETERS are defined here, with units. //precedes comments:
real gKleak= 0.0003 siemens/cm^2, //Permeant bkgd leak =10^6ch/cm^2
  gKstep= 0.0010 siemens/cm^2, //Max Perm for gated channel. One Siemen = 1/ohm
  Am = 1 cm^2, //Surface area of membrane
  Ko = 5 mM, Ki = 150 mM, // K concns outside and in
  R = 8.31441 J*mol^(-1)*K^(-1), // gas constant
  Temp = 310.16 K, //37C
  RT = R*Temp, //19.340*10^6 mmHg*cm^3*mol^(-1)at 37C
  Farad = 96485 coulomb*mol^(-1), //Faraday
  qe = 1.6022e-19 coulomb, //elementary charge
  //Nav= 6.0221e23, //Avagadro's #, no.molecules/mole
  kB =1.3807e-23 volt*coulomb*K^(-1), //Boltzmann's const., J*deg^-1
  RToF = (1000 mV/volt)*RT/Farad, //mV, RToF=26.73 mV at 37C,
  zg = 10, //# gating charges per channel
  boltzgz = (0.001 volt/mV)*zg*qe/(kB*Temp), //1/volt, RToF = kB*Temp/qe
  valence = 1, // boltcheck = qe/(kB*Temp),
  RTozF = RToF/valence, //RTozF = RT/(Farad*valence), mV;
  VK = 2.302585*RTozF*log(Ko/Ki), //mV, ENernst for K, mV
  EKchan= - 40 mV; //mean Em for chan opening, mV
// VARIABLES defined here, with units:
real Jelect(Em) amp; real zero(Em)=0; //zero(Em) is for plotting a level
// ODEs: //Area*(Siemens/Area)*V= Amp
  //gK = gKleak + gKstep/(1+exp(-boltzgz*(Em-EKchan))) siemens/cm^2;
  Jelect = Am*(Em-VK)*(gKleak + gKstep/(1+exp(-boltzgz*(Em-EKchan))));
}

```

For C, set the channel conductance to be at 50% open at  $-30$  mV. Set the leak conductance to a small value. Notice the slopes of the current voltage relationships in the different regions. For this result make the number of charges on the channel gate large to get a very sharp jump from closed to open.

For D, use a small number of charges on the channel gate. Try two different values for the voltage for 50% open. (Remember that each channel is either open or closed, so a conductance of 30% of maximum means that 30% of a large number of channels are open.)

**Nonlinear ionic conductances.** A problem with the linear current/voltage relationship of Eq. 7-8 is that not all channels demonstrate linearity. Linearity would be expected if electrochemical

gradient were the sole determinant. The local electric field within the channel, however, must also play a role, and voltage-dependent changes in the conformational state of the channel protein play an important role. What Goldman surmised is that the local strength of the electrical field must be a dominating influence, and on that basis he derived a solution for the simplest case, that of a linear gradient in potential along the channel, the constant field approximation, discussed in the next section.

The other problem created by having voltage-dependent conductivity is that the nice exponential relationship of Eq. 7-7 is no longer valid. Experimentally, this was approached by use of the “voltage clamp technique”, where the transmembrane voltage is held constant at chosen levels, and then step changes are made in the voltage in order to observe the currents. Since this leaves the prevailing electrochemical gradient as a driving force for current, the technique allows the examination of the conductance for a current at the moment after a voltage change, and allows the examination of the time course of the current decay at the chosen clamped voltage. If one clamps the transmembrane voltage at a level more positive than the Nernst potential, then a cation current will be outward; if one clamps at a level negative to the Nernst potential the cation current is inward. Thus at  $V(\text{clamp}) = 0$  mV, and using the cation concentrations given at the beginning of the chapter, a sodium current will flow inward, and a potassium current will flow outward.

### 7-3.3. The constant field approximation

A difficulty in applying the Nernst-Planck expression (Eq. 7-4) is in knowing the local, intramembrane gradients  $dC/dx$  and  $d\psi/dx$  through the membrane. The simplest approach, good enough for large pores where the effective diffusion coefficient is the same as in the bulk fluid, assumes a linear gradient (constant field), in which case the concentration  $C$  no longer represents the local concentration at a point but rather is the average within the pore,  $\bar{C} = (C_o + C_i)/2$ , where  $C_o$  and  $C_i$  are outside and inside concentrations, and  $\Delta x$  is membrane thickness or channel length:

$$J_s = -D \left( \frac{\Delta C}{\Delta x} + \frac{zF\bar{C}}{\mathfrak{R}T} \frac{\Delta\Psi}{\Delta x} \right), \quad (7-10a)$$

or using the definition for permeability,  $P = D/\Delta x$ ,

$$J_s = -P \left( \Delta C + \frac{zF\bar{C}}{\mathfrak{R}T} \Delta\Psi \right). \quad (7-10b)$$

Goldman (1943), rearranged Eq. 7-10a for the steady-state condition of constant flux:

$$0 = \frac{d}{dx} C + \frac{zF}{\mathfrak{R}T} \frac{\Delta\Psi}{\Delta x} C + \frac{J_s}{D}, \quad (7-11)$$

for which the solution is

$$\exp\left(\frac{-zF\Delta\Psi}{\mathfrak{R}T} \frac{x}{\Delta x}\right) C(x) = \frac{-J_s \mathfrak{R}T \Delta x}{D z F \Delta\Psi} \left[ \exp\left(\frac{-zF\Delta\Psi}{\mathfrak{R}T} \frac{x}{\Delta x}\right) - 1 \right] + C_1, \quad (7-12)$$

where the left or inside boundary condition is  $C(x=0) = C_1$ , and position  $x$  runs from 0 to  $\Delta x$ . The boundary condition at the right boundary is  $C(x=\Delta x) = C_2$ , the outside concentration. Then Goldman, assuming that the gradient was uniform (linear, the *constant field assumption*), and therefore that the gradients in  $\Psi$  and  $C$  were governed strictly by the conditions in the bulk phases on either side of the membrane, integrated across the membrane to get

$$J_s = -P\beta \frac{C_1 - C_2 e^\beta}{1 - e^\beta}, \text{ with } \beta = \frac{zF}{\mathfrak{R}T} \Delta\Psi = -\frac{zF}{\mathfrak{R}T} V. \quad (7-13)$$

$J_s$  is a net flux per unit surface area of a membrane, not a unidirectional flux.  $V$  is the transmembrane voltage  $\Psi_1 - \Psi_2$ ;  $\beta$  is dimensionless; the permeability  $P$  has units  $\text{cm/s}$ , so the flux  $J_s$  has the units of  $P$  times  $C$  or  $\text{mol s}^{-1} \text{cm}^{-2}$ . The fluxes for a range of  $\Delta\Psi$  and  $\Delta C$  are shown in Fig. 7-4 for a monovalent cation ( $z = +1$ ) for which the membrane permeability is  $10^{-5} \text{ cm s}^{-1}$ . Positive flux is from side 1 to side 2; with a ten-fold ratio of concentrations,  $C_1/C_2 = 10$ , the flux must be zero at the Nernst potential, at about +60 mV. With a ratio of 1, the Nernst potential is zero and with  $C_1/C_2 = 0.10$ , it is -60 mV. The slope of the line,  $J_s$  versus  $\Delta\Psi$  or  $J_s/\Delta\Psi$ , is determined by  $P$ ; Eq. 7-13 reduces to  $J_s = P(C_1 - C_2)$  when  $\Delta\Psi = 0$ . Although it seems highly unlikely that the field inside a membrane-spanning protein forming a channel should be linear, experimental observations on natural and artificial membranes made with a variety of concentrations and ions affirm the veracity of Eq. 7-13 and the applicability of the constant field assumption.

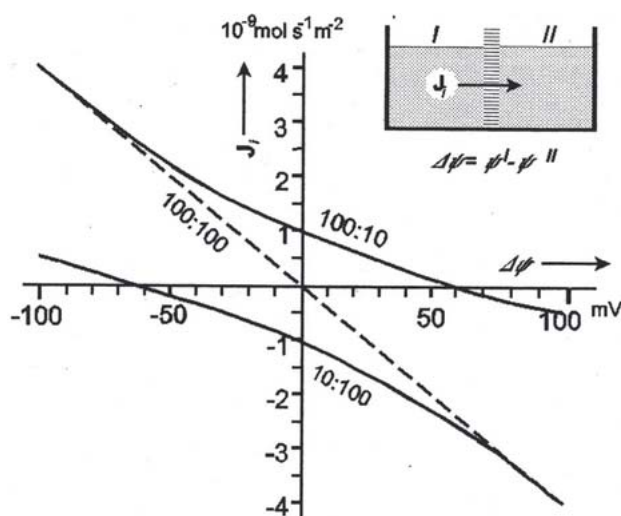


Figure 7-4: Flux versus transmembrane potential for a univalent cation using Eq. 7-13. See text. (Figure from Glaser, 2000, with permission.) The intercepts of the three curves on the voltage axis are the Nernst potentials for the individual cases.

The flux density  $J_s$ , with units moles per unit area per unit time is translated to a current by taking into account the number of charges per mole:

$$i, \text{ current density per unit area, amperes} \cdot \text{cm}^{-2} = zFJ_s, \text{ moles} \cdot \text{sec}^{-1} \text{cm}^{-2}. \quad (7-14)$$

Since the  $\beta$  in Eq. 7-13 contains  $zF$  already, this explains why the term  $z^2F^2$  often appears in current equations.

$$i = zF \cdot J_s = -\frac{(zF)^2}{\mathfrak{R}T} VP \frac{C_1 - C_2 e^\beta}{1 - e^\beta}. \quad (7-15)$$

#### 7-3.4. The case of a neutral particle

When  $z = 0$ , Eq. 7-13 and Eq. 7-3 both reduce to Fick's first law for diffusion in the presence of a concentration gradient:

$$\begin{aligned} J_s &= -\frac{C\mathfrak{R}T}{f_s \mathfrak{N}} \left( \frac{d \ln C}{dx} \right) \\ &= -\frac{C\mathfrak{R}T}{f_s \mathfrak{N}} \frac{dC}{C dx} = -\frac{\mathfrak{R}T}{f_s \mathfrak{N}} \frac{dC}{dx} = D \frac{dC}{dx}. \end{aligned} \quad (7-16)$$

From the expression for  $D$ ,  $D = \mathfrak{R}T/f_s \mathfrak{N}$ , from Stokes' Law for spherical molecules,  $f_s = 6\pi r\eta$ , and taking particular values, for  $r = 0.3$  nm and  $\eta = 1$  cP:

$$\begin{aligned} D &= \frac{\mathfrak{R}T}{6\pi r\eta \mathfrak{N}} = \frac{19.34 \times 10^6 (\text{mmHg} \cdot \text{cm}^3 \cdot \text{mol}^{-1}) \times 1333 (\text{g cm}^{-1} \text{s}^{-2} / \text{mmHg})}{6\pi 0.3 \times 10^{-7} (\text{cm}) 0.01 (\text{poise} = \text{g s}^{-1} \text{cm}^{-1}) 6.022 \times 10^{23} \text{mol}^{-1}} \\ &\approx 7.6 \times 10^{-6} \text{cm}^2 \cdot \text{s}^{-1}. \end{aligned}$$

This estimate of  $D$  is a good approximation for small solutes; it does slightly overestimate the diffusion coefficient for sucrose, which has a molecular radius of about 0.25 nm, and this is really to be expected since sucrose is a rough prolate ellipsoid, American football shape, not a sphere, and has an axial ratio of about two. (See Chapter 5, Frictional coefficients.) The sources of error can only be in the frictional coefficient because the rest of the terms are physical constants. (The hydrodynamic formulation itself may err; if the solute is not spherical  $f_s$  increases; particle flexibility usually reduces  $f_s$ , and the pore may not be a nice cylinder.) For other than unit area, the absolute flux  $j_s = -DA dC/dx$ , as before, and  $j_s = J_s \times A$ .

#### 7-4. The resting transmembrane potential, $E_R$

“Resting” means that the cell is not being stimulated or in the midst of an action potential. Currents flow, for there are almost always gradients and always leaks. The membrane potential is governed by the prior history (capacitance, ionic composition) and by the balance of inward and outward currents of charged solutes and ions. For most cells the resting transmembrane potential is governed mainly by the potassium potential since at this voltage (-10 to -80 mV depending on cell type) the conductivity for potassium is higher than for other cations, and chloride conductance is high and its distribution is passive. Because there is a transmembrane concentration difference maintained by the ATP-driven sodium-potassium exchange pump, the NaK ATPase, the situation is like the potassium-driven battery diagrammed in Figure 7-2. (The

-ase suffix signifies that ATP is hydrolyzed to provide the energy stored as a high energy phosphate bond to drive the pump.) The pump is electrogenic, meaning that operating it causes a potential to be generated across the cell membrane. The pump extrudes 3 Na<sup>+</sup> ions for each 2 K<sup>+</sup> ions carried into the cell, a stoichiometry of 3 to 2; the normal direction of the pump, driving more cations out than in, creates an imbalance with fewer cations inside than outside, and therefore creates an inside negative transmembrane potential. Muscle and nerve cells normally have resting potentials,  $E_R$ , of  $-70$  to  $-90$  mV, while epithelial and endothelial cells are observed to have  $E_R$ s of  $-20$  to  $-50$  mV.

**Problem.** If  $E_R$  is  $-90$  mV in a cardiac cell, and if all cation conductances except that for K<sup>+</sup> are zero, and  $[K^+]_o$  is 5 mM, what is the intracellular concentration  $[K^+]_i$ ? Use the Nernst equation.

#### 7-4.1. Goldman-Hodgkin-Katz expression for the resting potential

Eq. 7-13 was derived for a single ionic species, and would suffice for calculating the resting membrane potential if potassium were the only ionic leak or open channel. When more than one ion contributes to the membrane conductance, then all the currents must be collected together, accounting for the valence of each ion, and giving a net current of zero:

$$0 = \sum_j P_j \frac{c_i^j - c_e^j \exp\left(\frac{-zVF}{RT}\right)}{1 - \exp\left(\frac{-zVF}{RT}\right)}, \quad (7-17)$$

where  $P_j = D_j/\delta$ , the diffusion coefficient in the channel for the  $j^{\text{th}}$  ion divided by the channel length,  $\delta$ . Applying this to Na<sup>+</sup>, K<sup>+</sup>, and Cl<sup>-</sup> channels, an equation for the resting potential with zero net current is

$$E_R = \frac{RT}{F} \ln \left( \frac{P_{Na}[Na^+]_i + P_K[K^+]_i + P_{Cl}[Cl^-]_e}{P_{Na}[Na^+]_e + P_K[K^+]_e + P_{Cl}[Cl^-]_i} \right). \quad (7-18)$$

Unlike the Nernst Equation, which can be derived on thermodynamic principles, the Goldman-Hodgkin-Katz (GHK) expressions for currents and for the resting potential are derived through specific assumptions incorporated into the model for a constant field within the channel. Other models have been explored; this one's popularity is due to its simplicity; it is in practice pretty good. The chloride component is often omitted because chloride permeability is so high that chloride is usually in electrochemical equilibrium and does not influence the resting potential. Calcium leaks are relatively small and, while commonly ignored, can be incorporated into the expression, accounting for the valence of 2 (Sperelakis, 1979).

Other contributors to the  $E_R$  are, however, not to be neglected so easily. Equation 7-18 is for a steady state in which the chemical potentials are maintained and the leakage currents dominate. However, consider that in the same steady state, the maintenance of the imbalances in concentration is going on simultaneously and therefore there must be restoring currents of the same magnitude as the leaks. The dominant one is due to the sodium pump, the NaK ATPase, which is electrogenic since it drives out 3 Na<sup>+</sup> for each 2 K<sup>+</sup> it carries in. Lauger (1991) advocates

following Mullins and Noda (1963) to modify the GHK equation to account for the stoichiometry of the pump,  $r_p = 2/3$ , as follows:

$$E_R = \frac{RT}{F} \ln \left( \frac{P_{Na}[Na^+]_i + r_p P_K [K^+]_i}{P_{Na}[Na^+]_e + r_p P_K [K^+]_e} \right). \quad (7-19)$$

Another version makes good sense since the normal operation of the pump for net efflux, dependent on the pump rate, is to consider the ATPase current as an additional outward current like those for  $Na^+$  and for  $K^+$  and therefore to add it to the numerator of Eq. 7-18.

$$E_R = \frac{RT}{F} \ln \left( \frac{P_{Na}[Na^+]_i + P_K [K^+]_i + J_{pump} RT / (F E_R)}{P_{Na}[Na^+]_e + P_K [K^+]_e} \right). \quad (7-20)$$

This approach is discussed in detail by Sperelakis (1979). In Eq. 7-20,  $E_R$  appears on the right side as well as on the left, but since the pump current itself is small,  $E_R$  can be guessed approximately when solving the expression for the left side  $E_R$ , and the process iterated if the guess is not close enough. As Lauger (1991) pointed out, the pump current should not have more than a 10 mV influence in the steady state, but it is always hyperpolarizing when  $E_R$  is near  $E_K$  and has the possibility of pushing  $E_R$  to levels below  $E_K$ . Experimentally, poisoning the pump with ouabain reduces the membrane potential by about 8 mV, in accord with expectations.

Some interesting experiments have been done that illustrate the pump's remarkable power. An incidental observation in one of our studies (on the effects of raised  $[Ca]_i$  on  $P_K$ ; Bassingthwaite, Fry and McGuigan, 1974), in which cooling cardiac tissue to less than 10 C for several hours stopped the pump, and so loaded the cells with sodium, was that upon rewarming without stimulating the cells the membrane potential hyperpolarized from about -40 mV to below -120 mV as the pump extruded the excess sodium. A similar result was found in skeletal muscle upon resupplying external potassium after the intracellular sodium levels had risen during a few-hour period in low potassium and, even more interestingly, in fresh muscle tissue taken from hypokalemic rats when put into normal 5 mM  $K^+$  solutions (Akaike, 1979, and earlier papers). The most negative hyperpolarizing potentials reported are those by Tamai and Kagiya (1968); they found left ventricular muscle hyperpolarization to -260 mV during rewarming after sodium loading by prolonged cooling, although such high values have not been reaffirmed. The ATP-supported pump is driven by high intracellular sodium levels, so either the pump current strikingly overwhelms the leak currents and dominates the transmembrane potential, or the intracellular concentration is reduced below normal values; unfortunately the experiments don't apportion the importance of these two possible mechanisms.

**Problem.** If *all* cation and anion conductances except those for  $K^+$  and  $Na^+$  are zero,  $E_R = -80$  mV,  $[K^+]_o$  is 5 mM,  $[K^+]_i$  is 150 mM,  $[Na^+]_o$  is 140 mM, and  $[Na^+]_i$  is 14 mM, what is the ratio of the leakage currents? (Do this part in your head.) What is the ratio of ionic conductances  $P_{Na}/P_K$ ? (Answers: 1/14; less than 1/14, because the driving force for Na is much higher.??calc??)

## 7-4.2. Gibbs-Donnan equilibrium and the Donnan potential

The membrane potential at rest is not governed solely by the Nernst potentials of any open channels; it is also governed by the presence within the cell of charged species which cannot cross the membrane. The presence of impermeable solutes having a net charge causes an imbalance among the ionic solutes which can cross the membrane. In cells, the internal charge-carrying molecules are proteins, which generally have strongly negative net charges and therefore also buffer the positive charges, particularly  $H^+$ .

A Gibbs-Donnan equilibrium will be set up across a membrane when it is impermeable to one charged species but permeable to others. For a simple introductory example, put Congo Red,  $Na^+ R^-$ , in compartment A across a semipermeable membrane from  $NaCl$  in compartment B. The membrane is impermeable to the Congo Red,  $R^-$ , a large molecule, but is permeable to  $Na^+$  and  $Cl^-$ . Let the compartment volumes be equal,  $V_A = V_B$ :

$[Na^+]_{Ai}$	$[Na^+]_{Bi}$
$[R^-]_{Ai}$	$[Cl^-]_{Bi}$

Initially, let  $[Na^+]_{Ai} = [R^-]_{Ai} = 10 \text{ mEq/l}$ ,  $[Na^+]_{Bi} = [Cl^-]_{Bi} = 20 \text{ mEq/l}$ , where subscripts A and B indicate the compartment, the subscript  $i$  is initial, and  $f$  indicates final.  $Na^+$  and  $Cl^-$  can move to reduce the concentration gradient, but total electroneutrality must persist, i.e., for each  $Na^+$  that moves, a  $Cl^-$  must accompany it.

At equilibrium the membrane potential difference  $\Delta\Psi$  can be calculated in accordance with the Gibbs-Donnan equation for either  $Na^+$  or  $Cl^-$ , because the membrane is permeable to both:

$$\Psi_A - \Psi_B = \frac{RT}{zX_e} \ln(C_B/C_A).$$

$\Delta\Psi = (RT/X_e)(1/[+1]) \ln([Na^+]_B/[Na^+]_A)_f$  for sodium at final,  $f$ , steady state;  $\Delta\Psi = (RT/X_e)(1/[-1]) \ln([Cl^-]_B/[Cl^-]_A)_f$  for chloride and, putting these together,  $\ln([Na^+]_B/[Na^+]_A)_f = -\ln([Cl^-]_B/[Cl^-]_A)_f$ . Considering electroneutrality,  $Na_B = Cl_B$  and  $Na_A = Cl_A + R_A$ , then from  $(Na_B/Na_A) = Cl_B/(Cl_A + R_A)$ ,

$$\left( \frac{[Na^+]_B}{[Na^+]_A} \right)_f = \left( \frac{[Cl^-]_A}{[Cl^-]_B} \right)_f = \sqrt{\frac{[Cl^-]_{A_f}}{[R^-]_A + [Cl^-]_{A_f}}}, \quad (7-21)$$

the Gibbs-Donnan equation, the last term being obtained by substituting for  $C_B$ . Cross-multiplying the first two terms gives

$$[Na^+]_{B_f} \cdot [Cl^-]_{B_f} = [Cl^-]_{A_f} \cdot [Na^+]_{A_f}.$$

Since compartment volumes  $V_A$  and  $V_B$  are equal, and since very nearly equal amounts of  $Na^+$  and  $Cl^-$  are transferred (very little *net* charge is transferred in bringing about sizeable voltage changes), one can consider equal amounts,  $Y$ , to be transferred.  $Y$  can be calculated:

$$\begin{aligned}
 Y &= V_B([\text{Na}^+]_{B_i} - [\text{Na}^+]_{B_f}) = V([\text{Na}^+]_{A_f} - [\text{Na}^+]_{A_i}) \\
 &= V_B([\text{Cl}^-]_{B_i} - [\text{Cl}^-]_{B_b}) = V([\text{Cl}^-]_{A_f} - [\text{Cl}^-]_{A_i}) \quad .
 \end{aligned}$$

Use these to substitute for the final values in the Gibbs-Donnan equation:

$$([\text{Na}^+]_{B_i} - Y/V_B) \cdot ([\text{Cl}^-]_{B_i} - Y/V_B) = ([\text{Na}^+]_{A_i} + Y/V_A) \cdot ([\text{Cl}^-]_{A_i} + Y/V_A).$$

Initially,  $[\text{Na}^+]_{B_i} = [\text{Cl}^-]_{B_i}$  and  $[\text{Cl}^-]_{A_i} = 0$  in this case. Therefore,  $([\text{Na}^+]_{B_i} - Y/V_B) = ([\text{Na}^+]_{A_i} + Y/V_A) \cdot Y/V_A$ . Multiplying,

$$[\text{Na}^+]_{B_i}^2 - 2[\text{Na}^+]_{B_i} \frac{Y}{V_B} + \frac{Y^2}{V_B^2} = [\text{Na}^+]_{A_i} \frac{Y}{V_A} + \frac{Y^2}{V_A^2},$$

so that when  $V_A = V_B$  the  $X^2$  terms cancel and

$$\frac{Y}{V_A} = \frac{[\text{Na}^+]_{B_i}^2}{[\text{Na}^+]_{A_i} + 2[\text{Na}^+]_{B_i}} = \frac{400}{10 + 40} = 8. \quad (7-22)$$

Thus, finally,  $[\text{Na}^+]_{B_f} = 12$ ,  $[\text{Cl}^-]_{B_f} = 12$ ,  $[\text{Na}^+]_{A_f} = 18$ ,  $[\text{Cl}^-]_{A_f} = 8$ , with  $[\text{R}^-]_A$  unchanged at 10.

This equilibrium will be maintained only if the volumes of A and B are held constant. It is obvious that an osmotic gradient remains. The potential difference across the membrane is now (assuming equal activity coefficients in A and B)

$$d\Psi = \frac{RT}{ZF} \log_e \left( \frac{[\text{Na}^+]_{B_f}}{[\text{Na}^+]_{A_f}} \right) = \frac{58}{(+1)} \log_{10} \left( \frac{12}{18} \right) \text{ millivolts} = 23.5 \text{ mv}.$$

**Problem.** The problem, a complicated one, is to find a transient and steady-state solution accounting for both osmolarity and charge. Try writing the differential equations for solutes, solvents and electrical potential difference, given a pressure-volume relationship for the cell. Consider two extreme cases, one solving for  $\Delta p$  for completely rigid cells A and B, one for completely distensible cells in which no  $\Delta p$  is generated, and a third case using an intermediate degree of stiffness allowing changes in volume and pressure. The existence of a Donnan potential does not depend on the presence of a cell membrane, but only on the maintenance of a region where there is protein or charged gel distinguished from a surrounding solution.

**Problem.** If you should fail to find a steady-state solution to the previous problem, discuss why this might be. How would you design the cell in order to reach a steady state?

## 7-4.3. Electrodiffusion

## 7-4.3.1. An example problem with its answer

Consider the flux of a dissociated uni-univalent salt in an electric field along an open pore traversing a membrane.

Take the following one-dimensional equation for flux per unit area of an ion in a solution:

$$J_i = u_i C_i \left( \frac{-RT}{z_i F} \frac{\partial}{\partial x} \ln C_i + \frac{\partial \Psi}{\partial x} \right) + J_v C_i. \quad (7-23)$$

1. Identify all symbols, and give units. (Hint: See Chapter 1, Terminology.)
2. What changes, if any, would be required to make the equation applicable to charged membranes? (Hint: Integrate across the membrane to define  $\Delta C$  and  $\Delta \Psi$ .)
3. Apply the equation to the diffusion of a single uni-univalent salt in the absence of convection. Obtain an expression for (1) the electrical potential difference produced, and (2) the flux of the salt.
4. Still with reference to a single uni-univalent salt, consider the situation in which the mobility of the anion is zero. What will be the expression for (1) the potential difference, and (2) the flux of the cation? What physical conditions might cause the mobility of the anion to be zero in a porous membrane?
5. Show how this equation reduces to Fick's first law when applied to the diffusion of a nonelectrolyte in the absence of convection.

## 7-4.3.2. Answers to the question

**a. Identify all symbols.** The equation, Eq. 7-23, is for flux per unit surface area,  $J_i$ , of an ion in the  $x$  direction and gives the sum of fluxes due to diffusion (first term on right), due to electrical field (second term on right), and due to convection of the solution itself (third term).

$u_i$  is the mobility within the channel (velocity per unit voltage gradient in  $\text{cm s}^{-1}/(\text{V}/\text{cm})$ ),  
 $C_i$  is concentration (millimoles/ $\text{cm}^3$  or M),  
 $R$  is the gas constant (0.082 liter atmos/(mol deg K) or 8.31441 Joules  $\text{mol}^{-1}$  deg $^{-1}$ ),  
 $T$  is the temperature (deg K),  
 $z_i$  is valence, +1 and -1 in this case,  
 $F$  is Faraday's constant (96484 coulombs/mol),  
 $\Psi$  is the electric potential (volts),  
 $J_i$  is the ion flux ( $\text{mol}/(\text{s cm}^2)$ ),  
 $J_v$  is the volume flux, solvent + solute ( $\text{ml}/(\text{s cm}^2)$ ),  
 $x$  is distance (cm).

The subscript  $i$  refers to the  $i^{\text{th}}$  species; "ln" refers to logarithm to the base  $e$ .

**b. What changes need to be made if the membrane is charged?** None really, except that specifying the conditions at either side of the membrane may help to simplify the problem by defining  $\Delta C$  and  $\Delta \Psi$  at those points. The equation is applicable to charged membranes in the current form. However if there were charges within the internal structures of the membrane, these

might affect the diffusivity or mobility of the solute through the membrane. For convenience, we can rewrite the equation in the question as

$$J_i = -D_i \frac{\partial C_i}{\partial x} + u_i C_i \frac{\partial \Psi}{\partial x} + J_v C_i, \quad (7-24)$$

where we have used the Einstein relation:

$$D_i = \frac{u_i RT}{z_i F}. \quad (7-25)$$

This diffusion coefficient is the same as the diffusion coefficient in the bathing solutions only if there is no steric hindrance or local charge density effect within the membrane, that is, the reflection coefficient is zero. Note the relationship to the Einsteinian diffusion coefficient given in Eq. 7-25 as compared with that given in Chapter 5 for uncharged spherical particles:

$$D_i = \frac{RT}{6\pi r \eta N_A}. \quad (7-26)$$

**c. Uni-univalent salt in the absence of convection.** If we assume that there is no net electrical current (that is, the system is open), then the flux of anion and cation must be equal:  $J_- - J_+ = 0$ . Using Equation 7-24 for each ion and using  $J_+ = J_-$ , which is true after a brief moment even if their mobilities differ, gives

$$-D_+ \frac{\partial C_+}{\partial x} + D_- \frac{\partial C_-}{\partial x} + [u_+ C_+ - u_- C_-] \frac{\partial \Psi}{\partial x} = 0, \quad (7-27a)$$

where the ion concentrations are defined by

$$C_+ = C_o + \tilde{C}_+ \quad \text{and} \quad (7-27b)$$

$$C_- = C_o + \tilde{C}_-, \quad (7-27c)$$

where  $C_o$  is the bulk salt concentration. Since both  $\tilde{C}_i$  must be much smaller in magnitude than  $C_o$  to preserve charge neutrality, then  $C_+$  is nearly equal to  $C_-$  and both are equal to  $C_o$ . Then Equation 7-27a reduces to approximately

$$\frac{\partial \Psi}{\partial x} = -\frac{(D_+ - D_-)}{(u_+ - u_-)} \cdot \frac{\partial C_o}{\partial x}. \quad (7-28)$$

Integration over distance 0 to  $x$  gives

$$\Psi(x) = -\frac{(D_+ - D_-)}{(u_+ - u_-)} \log\left(\frac{C_o(x)}{C_o(0)}\right), \quad (7-29)$$

if we define the potential at  $x = 0$ ,  $\Psi(0)$ , to be zero. Using the Einstein relation for the mobility and accounting for the valences, we get

$$\Psi(x) = -\frac{RT(D_+ - D_-)}{F(D_+ + D_-)} \log\left(\frac{C_o(x)}{C_o(0)}\right). \quad (7-30)$$

Therefore the potential drop (excluding any boundary layers where  $|\tilde{C}_i|$  may not be small compared to  $|C_o|$ ) is given by

$$\Delta\Psi_{\text{diff}} = -\left(\frac{RT}{F}\right)\frac{(D_+ - D_-)}{(D_+ + D_-)} \log\left(\frac{C_o(x)}{C_o(0)}\right). \quad (7-31)$$

We label this  $\Delta\Psi_{\text{diff}}$  a *diffusion potential*, because it is the potential that is due to differences in diffusibility or mobility of the two mobile species. If the mobilities are equal, then  $\Delta\Psi_{\text{diff}} = 0$ ; this is the case for KCl, and is the basis for its use in electrodes: KCl electrodes have almost no artifact in measured voltage due to diffusion potential, because the diffusion coefficients for  $\text{K}^+$  and  $\text{Cl}^-$  are so close,  $1.96$  and  $2.0 \cdot 10^{-5} \text{ cm}^2/\text{s}$  at  $25 \text{ C}$ .

To find the flux of salt we need to return to Eq. 7-2. For a uni-univalent electrolyte we get

$$J_+ = -D_+ \frac{\partial C_+}{\partial x} + u_+ C_+ \frac{\partial \Psi}{\partial x}, \quad (7-32)$$

$$J_- = -D_- \frac{\partial C_-}{\partial x} - u_- C_- \frac{\partial \Psi}{\partial x}. \quad (7-33)$$

We can take the gradient of each of these equations to get

$$\frac{\partial C_+}{\partial t} = -D_+ \frac{\partial^2 C_+}{\partial x^2} + u_+ \frac{\partial}{\partial x} \left( C_+ \frac{\partial \Psi}{\partial x} \right), \quad (7-34a)$$

$$\frac{\partial C_-}{\partial t} = -D_- \frac{\partial^2 C_-}{\partial x^2} - u_- \frac{\partial}{\partial x} \left( C_- \frac{\partial \Psi}{\partial x} \right). \quad (7-34b)$$

If we multiply Equation 7-34a by  $D_+$  and Equation 7-34b by  $D_-$  and add the two together we get

$$\frac{\partial}{\partial t} (D_+ C_+ + D_- C_-) = D_+ D_- \frac{\partial^2}{\partial x^2} (C_+ + C_-) - \frac{\partial}{\partial x} \left( \frac{zF}{RT} D_+ D_- (C_+ - C_-) \frac{\partial \Psi}{\partial x} \right). \quad (7-35)$$

If it can be shown that

$$\left| \frac{D_+ D_- (C_+ - C_-) \frac{\partial \Psi}{\partial x}}{\frac{RT}{zF} D_+ D_- \frac{\partial}{\partial x} (C_+ + C_-)} \right| \ll 1, \quad (7-36)$$

then Equation 7-35 reduces to

$$\frac{\partial C_o}{\partial t} = D_e \frac{\partial^2 C_o}{\partial x^2}, \quad (7-37)$$

where the effective diffusion coefficient  $D_e$  is given by

$$D_e = \frac{2D_+ D_-}{D_+ + D_-}. \quad (7-38)$$

Then, inequality expressed in Equation 7-36 can be approximated by

$$\left| \left( \frac{(\Psi^{\text{right}} - \Psi^{\text{left}})L}{(2RT)/(zF)} \right) \left( \frac{\rho_u}{\rho_o} \right) \right| \ll 1, \quad (7-39)$$

where  $\rho_u$  is the net charge density (positive minus negative) and  $\rho_o$  is the total charge density (positive plus negative). Equation 7-39 will be true for almost all cases of biological interest. Then the flux of the salt can be given by

$$J_o = -D_e \frac{\partial}{\partial x} \bar{C}_o \approx D_e \left( \frac{C_o^{\text{right}} - C_o^{\text{left}}}{L} \right). \quad (7-40)$$

When the membrane is not charged but there is a charge difference across the membrane, an alternative answer is that cation flux = anion flux (to preserve electroneutrality),

$$J_o = J_- + J_+. \quad (7-41)$$

Then the charge fluxes identified from Equation 7-32 and Equation 7-33 can be rewritten:

$$J_+ = -\mu_+ \cdot C_+ \cdot \left( RT \cdot \frac{d}{dx} \ln C_+ + F \cdot \frac{d\Psi}{dx} \right), \quad (7-42)$$

$$J_- = \mu_- \cdot C_- \cdot \left( RT \cdot \frac{d}{dx} \ln C_- - F \cdot \frac{d\Psi}{dx} \right). \quad (7-43)$$

Since  $J_- = J_+$ , and  $C_- \approx C_+ = C_o$ , the concentration of the salt, then

$$\frac{d\Psi}{dx} = -\frac{RT}{F} \cdot \frac{u_+ - u_-}{u_+ + u_-} \cdot \frac{d}{dx} \ln C_o. \quad (7-44)$$

Finally, the potential difference between the two bulk solutions of concentrations  $C_1$  and  $C_2$  obtained by integrating from side 1 to side 2 is

$$\Delta\Psi = \Psi_2 - \Psi_1 = -\frac{RT}{F} \cdot \left( \frac{u_+ - u_-}{u_+ + u_-} \right) \cdot \ln(C_2/C_1), \quad (7-45)$$

and  $\Delta\Psi$  will be positive if the cation moves faster than the anion, and vice versa, or will be zero if anion and cation have the same mobility. The flux calculation, accounting for electroneutrality, is obtained by substituting the  $d\Psi/dx$  of Equation 7-44 into Equation 7-42 and Equation 7-43:

$$J_o = -(u_+ + u_-)C_o \cdot \left( RT \frac{d}{dx} \ln C_o + \frac{FRT}{F} \cdot \frac{(u_+ - u_-)}{(u_+ + u_-)} \cdot \frac{d}{dx} \ln C_o \right), \quad \text{or} \quad (7-46)$$

$$J_o = J_+ + J_- = -RT \cdot \left( \frac{2u_+ u_-}{u_+ + u_-} \right) \cdot \frac{dC_o}{dx}. \quad (7-47)$$

**d. Mobility of the anion is zero.** *First the simple answer:* This answer assumes that there are no internal charges within the membrane, but that there is a potential difference across the membrane. From Equation 7-45, by putting the anion mobility to zero, the solute flux is forced to zero after the tiniest flux and we get the transmembrane potential due to the permeability to the univalent *cation* with  $z_i = 1$ , its Nernst potential:

$$\Psi_2 - \Psi_1 = -\frac{RT}{z_i F} \cdot \ln(C_2/C_1). \quad (7-48)$$

For example, with potassium concentration inside a cell at 150 mM and outside at 5 mM, and with potassium permeability high compared to all other ions, then  $C_2/C_1 = 30$  and the inside potential is about  $-60$  times  $\log_{10}30$  or  $-90$  mV. (See Chapter 1, Terminology, for the conversions in the units.) The cation flux goes to zero as soon as the Nernst potential is reached:  $J_+ = 0$ .

*Then a more detailed answer:* Assume that the mobility of the anion is finite in the bulk solvent and only becomes zero within the membrane.

In this case we cannot invoke electroneutrality inside the membrane because the anion cannot diffuse into the membrane to balance the charge. Therefore we cannot use the Donnan potential calculations. If we assume that electrolyte concentrations are governed by Boltzmann statistics (which assumes we are close to thermodynamic equilibrium), we get

$$C_+ = C_o e^{-F\Psi(r)/RT}, \quad (7-49)$$

$$C_- = C_o e^{F\Psi(r)/(RT)}, \quad (7-50)$$

where  $r$  denotes the distance from the interface and  $C_o$  is the bulk concentration in the solvent far away from the interface where the potential is defined to be zero. From Gauss's law we get

$$\frac{\partial^2 \Psi}{\partial r^2} = \frac{\rho}{\epsilon}, \quad (7-51)$$

where  $\rho$  is the charge density in the solution, Coulombs/cm<sup>3</sup> (or =  $C_i \cdot F$ ), and  $\epsilon$  is the dielectric constant of the solution. Substituting Equation 7-49 and Equation 7-50 into Equation 7-51 we find

$$\frac{\partial^2 \Psi}{\partial r^2} = \frac{2C_o}{\epsilon} \sinh\left(\frac{F\Psi(r)}{RT}\right), \quad (7-52)$$

which is known as the Poisson-Boltzmann equation. Equation 7-52 is nonlinear and difficult to solve. If we linearize it for small potentials we get the linearized Poisson-Boltzmann equation:

$$\frac{\partial^2 \Psi}{\partial r^2} = \frac{2C_o}{\epsilon} \left(\frac{F\Psi(r)}{RT}\right), \quad (7-53)$$

which has the solution

$$\Psi(r) = \Psi_o e^{-kr}, \quad (7-54)$$

where  $k^2 = 2C_o F / \epsilon RT$  and  $1/k$  is known as the Debye length. We can find  $\Psi_o$  from electroneutrality at the interface, which gives

$$\Psi_o = \frac{RT}{F} \sinh^{-1}\left(\frac{F\rho_m}{2C_o}\right). \quad (7-55)$$

Therefore the potential in the solvent is given by

$$\Psi(r) = \frac{RT}{F} \sinh^{-1}\left(\frac{F\rho_m}{2C_o}\right) e^{-kr}. \quad (7-56)$$

The potential drop across the interface is given by

$$\Delta\Psi_i = \frac{RT}{F} \sinh^{-1}\left(\frac{F\rho_m}{2C_o}\right) \approx \frac{1}{2} \frac{RT}{F} \log\left(\frac{F\rho_m}{C_o}\right). \quad (7-57)$$

The potential drop across both interfaces can then be given by

$$\Delta\Psi_i \approx -\frac{RT}{F} \log\left(\frac{C_o^{\text{right}}}{C_o^{\text{left}}}\right). \quad (7-58)$$

Since the cation concentration will be vanishingly small at each interface (from Equation 7-49) the ion concentration will be vanishingly small inside the membrane, and there will be no drift field inside the membrane. So the total potential drop will be

$$\Delta\Psi_{\text{total}} \approx -\frac{RT}{F} \log\left(\frac{C_o^{\text{right}}}{C_o^{\text{left}}}\right). \quad (7-59)$$

To find the flux we use

$$J_+ = D_+ \frac{\bar{C}_+^{\text{left}} - \bar{C}_+^{\text{right}}}{L} = \frac{D_+}{L} \left( \exp\left(-\sinh^{-1}\left(\frac{F\rho_m}{2C_o^{\text{left}}}\right)\right) - \exp\left(-\sinh^{-1}\left(\frac{F\rho_m}{2C_o^{\text{right}}}\right)\right) \right), \quad (7-60)$$

which can be approximated by

$$J_+ = \frac{D_+ F \rho_m}{2L} \left( \frac{1}{C_o^{\text{right}}} - \frac{1}{C_o^{\text{left}}} \right), \quad (7-61)$$

which will typically be very small.

**e. Reduction to the Fick's first law.** From the original expression, Eq. 7-46, considering  $d\Psi/dx = 0$ ,  $J_v = 0$ ,  $u = z_i F D / RT$ , and  $C d \ln C / dx = dC / dx$ , we get

$$J_i = u_i \frac{RT}{z_i F} \cdot \frac{\partial C_i}{\partial x} = D_i \cdot \frac{\partial C_i}{\partial x}, \text{ Fick's first law.} \quad (7-62)$$

## 7-5. Patch clamp studies of single-channel kinetics

The single-channel kinetics depicted in Figure 7-3 and calculated in the program in Table 7-3 represent what is observed when there are many channels in parallel; the resultant currents are the sum of the currents through the assemblage of channels, some of which are open and others, closed. The basic Boltzmann equation, Eq. 7-9, describes the *probability* of an individual channel being open at a given voltage; it does not specify how long it will remain open, only the fraction of time that it will be open. Sakmann and Neher (1983,1995) pioneered the development of the patch clamp technique for observing one channel protein at a time, for which they were awarded a Nobel prize. Observations of a single channel, maintained though the clamping of a tiny patch of cell membrane to chosen transmembrane voltages, reveal that the channel fluctuates between opening and closing, as in Fig. 7-5. Because the concentrations of  $\text{Na}^+$  are not changing, the currents are the same with each opening. There are no partially open states. The open-state current flow has the same form as in Eq. 7-8:

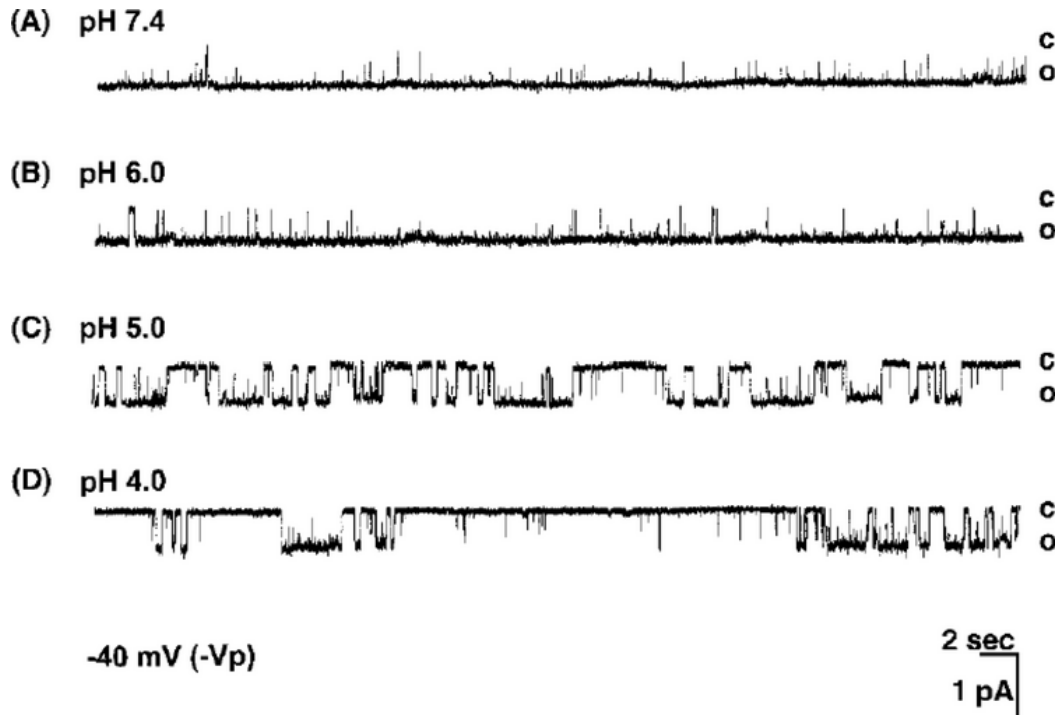


Figure 7-5: Single channel openings and closings as revealed by patch clamp of an epithelial  $\text{Na}^+$  channel expressed in a frog oocyte after injection of cRNA for the channel protein. The patch was held at a transmembrane potential of  $-40$  mV. The channel opening is almost 100% at pH 7.4 and diminishes to about 25% at pH 4.0. (From Zhang et al. 1999, their Figure 8, with permission.)

$$I = \frac{E_m - E_{\text{Na}}}{R} = g_{\text{Na}}(E_m - E_{\text{Na}}), \quad (7-63)$$

where  $g_{\text{Na}}$  is now the single-channel open conductance, usually a few picoSiemens. The opening probability can be measured, after holding the transmembrane voltage constant for a second to two to reach steady state, from the fraction of time that the channel is open. From the data obtained over a wide range of voltages one can construct curves of the form shown in Eq. 7-9 and so estimate the voltage for 50% open probability,  $E_{\text{Nachan}}$ , and the number of gating charges per channel,  $z_g$ .

The current-voltage relationships for the particular type of Na channel expressed in the oocytes used by Zhang et al. (1999) were linear, as demonstrated in whole cell currents, but had slopes dependent on the pH. As shown in Fig. 7-6, the current was maximal at high pH and was reduced by lowering extracellular pH. The response to a change in pH was very fast, and was therefore attributed to an  $\text{H}^+$  ion binding at an external site. The Hill coefficient was 1.0, indicating single-site binding. Background for this is in Chapter 6-10.

While Eq. 7-9 implies that when the voltage is stepped to a new level the channel protein changes shape instantly, one can appreciate that it inevitably takes some time for a channel protein to adapt to the changed voltage field. The simplest case occurs when the relaxation from one shape to another changes in proportion to the difference between the past state and the steady-state shape at the new voltage, for which the lag observed from a current change when

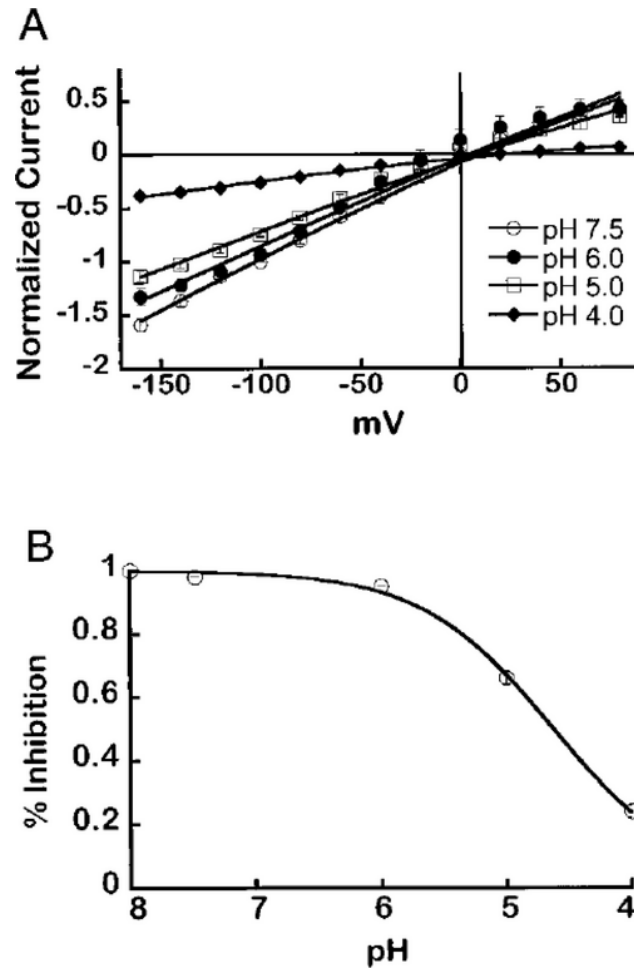


Figure 7-6: Whole cell current-voltage relationships for epithelial Na channels expressed in frog oocytes. At high pH all are open, but are inhibited by lowering extracellular pH. “Inhibited” means that opening times are reduced, as was observed in the patch clamp data in Fig. 7-5. The solid line is for a Hill-type equation for current  $I$  relative to its maximum,  $I/I_{\max} = 1/(1 + [H^+]/pK_a)^N$ , with  $N=1$  for single-site binding and  $pK_a = 4.6$ . (From Zhang et al. 1999, their figure 3 corrected, with permission.)

many channels are operating will be an exponential function with time constant  $\tau$ . Obtaining the time constant using single-channel patch clamp techniques requires averaging over many step responses, so it is easier to find time constants by using voltage clamp on a whole cell where there are many channels, and the observed currents give the average behavior. Then the steady-state opening probability will change:

$$P_{\text{open}}(t) = P_{\text{open}}(E_{\text{newSS}}) - [P_{\text{open}}(E_{\text{newSS}}) - P_{\text{open}}(E_{\text{oldSS}})] \cdot e^{-t/\tau}. \quad (7-64)$$

The time constant  $\tau$  is ordinarily dependent on the voltage; when voltage is changing continuously, as it does with each action potential *in vivo*, then  $P_{\text{open}}(t)$  changes continuously following the expected voltage-dependent steady-state value with a lag of  $\tau(E)$ . This is applying a first-order lag filter to  $P_{\text{open}}(t)$  with a voltage-dependent lag time.

Channel openings and closings are the result of sometimes fairly complex changes in conformational state, and there may be a variety of different states that are either open or closed. When there are only two states, open or closed, but it takes time for the conversion from one to the other, then the channel can be considered as a two-state Markovian system for which the Boltzmann expression needs modification to account for the time lag. The time lags normally take milliseconds and are dependent on voltage, something we will examine in detail later when describing the Hodgkin-Huxley action potential.

More complexity is common, for there may be multiple conformational states. When multiple states exist and the energy barriers between adjacent states are small, then these also influence the kinetics. An example is the observation of fractal kinetics for some potassium channels. Cole and Moore (1960) observed that the  $K^+$  channel of the squid axon appeared to have a large number of states, up to 25; this was surmised from the shape of the foot of the action potential. Liebovitch (1989) observed that  $K^+$  channels exhibited a peculiar statistical behavior when observed individually by patch clamp: there was a long-memory correlation structure in the time series of openings and closings, namely that long opening durations tended to be followed by another opening of long duration, and short opening durations tended to be followed by short opening durations. Statistically, processes with such behavior are termed long memory processes (Bassingthwaite, Liebovitch and West, 1994; Beran, 1994); these statistics show power-law correlation, i.e., the degree of correlation falls off as a function of time, observed as a straight line on a plot of log correlation versus log time lag for the correlation in the autocorrelation function. These intriguing observations lend credence to the principle that in general one may expect multiple conformational states. While the case for applicability to some  $K^+$  channels is reasonably good, most appear to be Markovian, i.e., most have two or very few states. The classic Na channel appears to have four states with similar characteristics over many phyla, and is discussed in the next section.

Multiple conductance levels are observed in some instances. This appears to be due to interaction between channels when they cluster together. Clustering of integral proteins is common, and is the usual thing for gap junctional connections between cells where they form hexagonal arrays (cardiac myocytes) or strings like spot welds (in endothelial junctions in continuous capillaries). An example of cooperativity is seen even in an artificial lipid bilayer to which was added a channel-forming toxin. In this case, the analysis of the individual channel conductance is more complex, as summarized in Fig. 7-7. The estimation of the three conductance levels is accomplished by fitting the observed histograms of numbers of instances of a particular voltage versus current with an assumed number of Gaussian distributions of currents, in this case four. The number isn't arbitrary but is constrained by the data, in particular by the form of the hump for current level 3 in the middle panel.

The pore characteristics of the beticolin 3 channel were explored by Goudet et al. (1999) by using non-electrolyte solutes at high concentration (20% weight/volume) to partially obstruct the flux of charge-carrying ions. The solutes were glucose (hydrodynamic radius 0.37 nm), sorbitol (0.39 nm), sucrose (0.47 nm), and a sequence of polyethylene glycols of increasing hydrodynamic radii, the larger of which could not enter the pore. The apparent channel conductances, shown in Fig. 7-8 A, diminish when non-electrolytes with radii less than about 0.75 nm obstruct current flow through the pore. Since this pore size indicator was the same for all three conductance levels, we conclude that the pores remain independent of one another so far as channel size is concerned. The chemical nature and structure of the beticolin 3 are shown in Fig. 7-8 B and C. The ratio of width to height being a little less than 1/2 would suggest that the

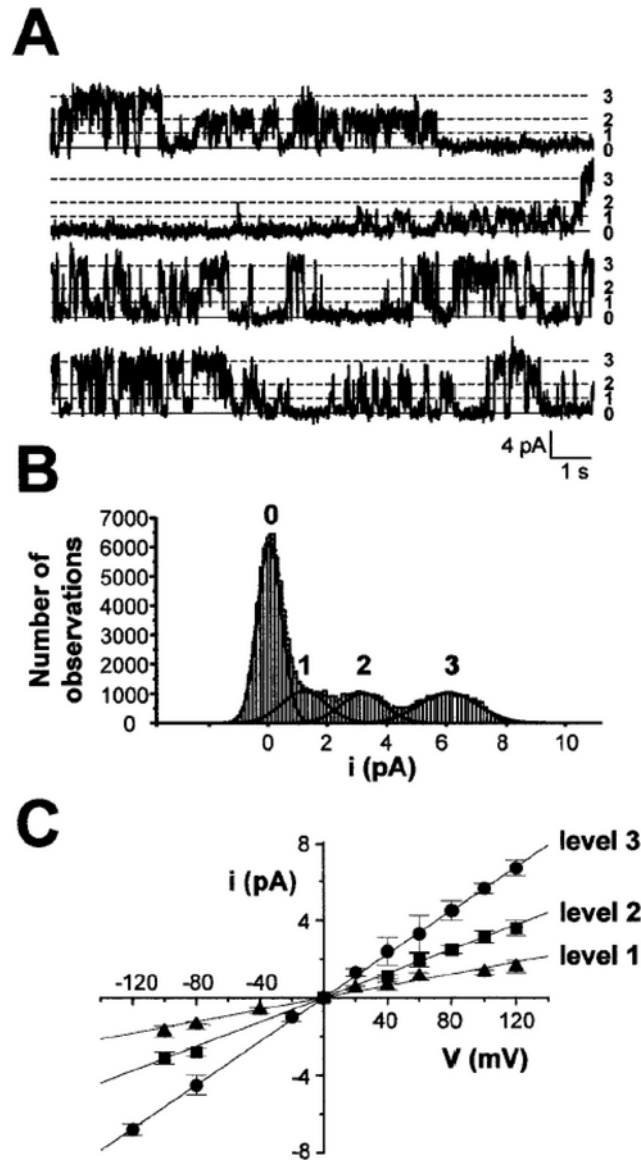


Figure 7-7: Toxin (beticolin 3) channels in an artificial lipid bilayer show three conductance levels, presumably due to near-neighbor cooperative interaction between toxin molecules in clusters. *Upper panel*: Patch clamp currents due to  $K^+$  flux in 200 mM  $K^+$  solution at membrane potential +100 mV. The three levels are indicated. *Middle panel*: Histograms obtained by time-binning are fitted with a sum of four Gaussian distributions. *Lower panel*: Mean current voltage relationships for the three open states for  $K^+$ . The channels were slightly ion selective, in the order  $Na^+ > Li^+ > K^+ > NH_4^+ > TEA^+ > Cl^-$ , the order being the same at all three conductance levels, and indicating that the individuality of each channel was maintained and that channels did not coalesce to enlarge the central passage. (From Goudet et al. 1999, their Figure 2, with permission.)

molecules must align with the channel to enter, and that they cannot rotate freely within it. The  $Mg^{2+}$  atoms and the oxygens and the size presumably determine the ion selectivity, though it is small.

## 7-6. The action potential in excitable cells

### 7-6.1. Neuronal currents

In excitable cells an action potential is initiated by a depolarizing current. When the degree of depolarization is sufficient it leads to an increase in the conductance of an ion, usually  $Na^+$  or  $Ca^{2+}$ , the influx of which into the cell leads to yet further depolarization, a “regenerative depolarization”, a prime example of positive feedback.

The nerve action potential was researched and analyzed beautifully by Hodgkin et al. (1952a,b,c,d,e) following the pioneering work of Hodgkin and Katz (1949) and Cole and Curtis (1939) and Curtis and Cole (1940, 1942), and is reviewed by Hille (1984, 2001). It serves as a relatively simple illustration of the time- and voltage-dependence of ionic currents when the membrane potential is perturbed. Every one of them is directly reproducible from the text and legends. Since many cell types, and probably at least some of all multicellular species, are excitable, and the excitation is key to neural control and to contractile cells and therefore to motion and function, the processes of excitation and its sequelae are central to biology. The experiments and analyses of Hodgkin and Huxley represent a masterful examination of a transmembrane current carrier, using systematic quantitative modeling, and the work won the Nobel Prize. The 1952e paper of Hodgkin and Huxley is not merely a beautiful summary of the work: it also provides a pioneering example of how to present a model paper, complete with the reporting of the parameters used for every figure.

Cole's work showed that the membrane impedance, the resistance to current flow, diminished greatly during the nerve action potential. The action potential was well underway before the membrane conductance (the height of the white area in Fig. 7-9) reached its peak. Cole and his colleagues did not identify the current carriers. What one would say now is that the conductance signal represents the sum of all the conductances (open channels) at each moment, so the data from Cole and Curtis (1939) should be explained by the sums of the conductances of all of the channels open at that moment. It is the differentiation and characterization of two distinctly different channel conductances by the Hodgkin and Huxley analysis which was so prescient.

See Bezanilla's website at UCLA (currently <http://pb010.anes.ucla.edu/>) for a good introduction to the Hodgkin-Huxley nerve action potential.

The task for Hodgkin and Huxley was to explain a broad set of observations not previously understood: (1) the basis of the conductance changes during an action potential, (2) the carriers for the current or currents, (3) the mechanism by which the action potential was propagated along the nerve axon, and (4) the quantitative basis for the speed of axonal propagation. It was known that the membrane had a high capacitance, astoundingly high compared to expectations. It was recognized that the action potential did not merely reduce the membrane potential to zero, but went into positive values; this was a big hint that more than one ion was involved. Hille (2001) and Keener and Sneyd (1998) delve into the history. The studies on the squid giant axon opened the floodgates and gave rise to a surge of research scarcely paralleled until recently with the great stimulus of genomics. After the H-H nerve was elucidated, cardiac action potentials soon followed (Weidmann, 1956; Noble, 1962). Single-cell studies didn't really succeed, with the

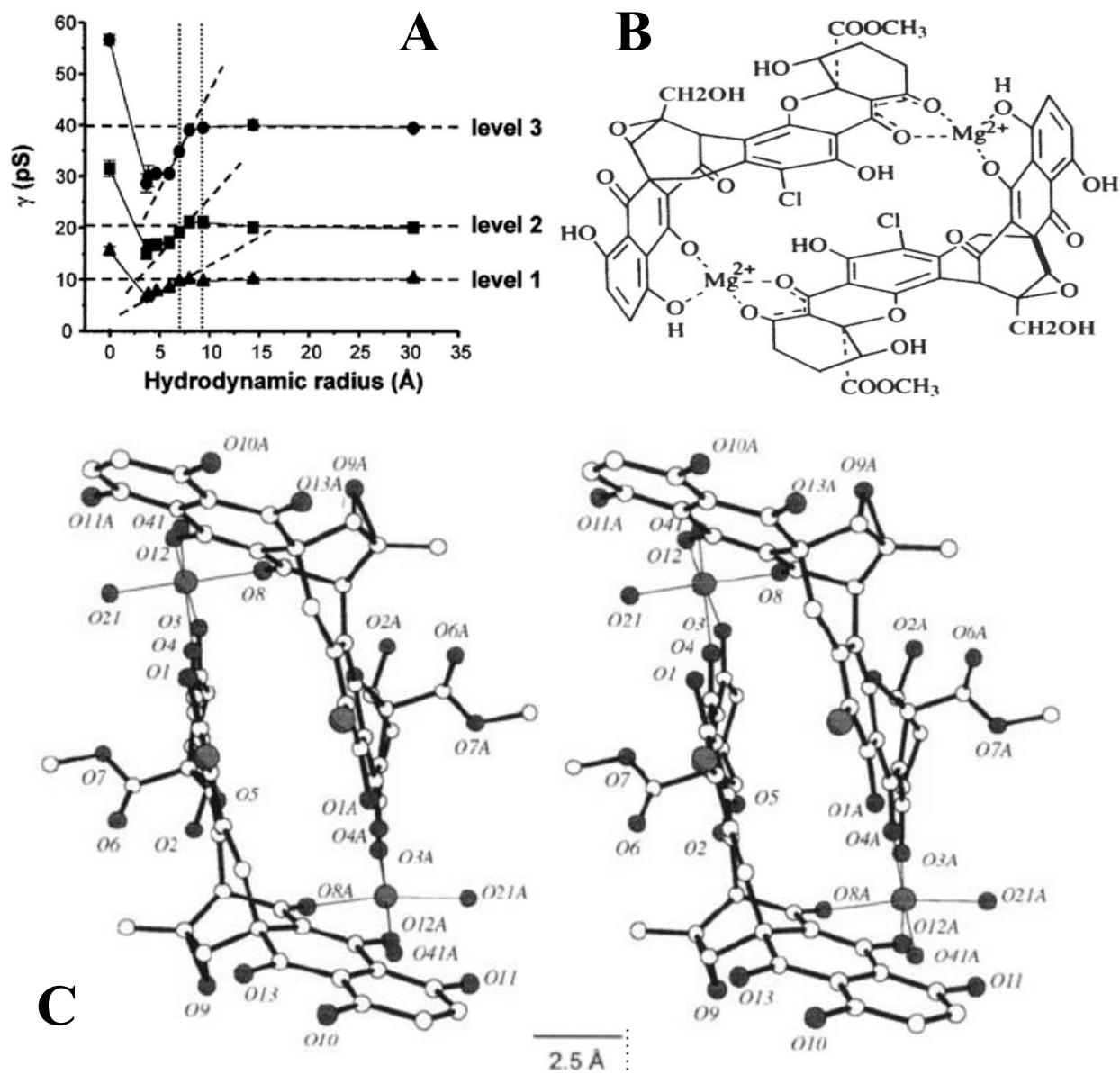


Figure 7-8: Beticolin dimer channel. *Panel A*: Conduction of pore is reduced by neutral molecules filling the pore. Reduction of ionic conductance by neutral solutes of differing size indicates a pore size of about 0.75 nm. *Panel B*: Molecular structure of beticolin 3 dimer forming a channel. *Panel C*: Stereo view of the beticolin 3<sup>-</sup> Mg<sup>2+</sup> dimer showing a rectangular pore of about 0.3 by 0.8 nm. The monomers are linked through the Mg<sup>2+</sup> - O<sub>2</sub> attraction. The stereo view, C, shows that the rectangular space is lined with polar oxygens and the two Mg<sup>2+</sup>. (From Goudet et al. 1999, their Figures 4 and 6, with permission.) [One way to see the stereo view is to center one's nose about 10 inches from the picture, with eyes looking straight ahead and focusing through the center of the picture between the two views of the molecule to about 10 inches behind the page. Relaxing the eyes helps the three-dimensional picture to emerge.]

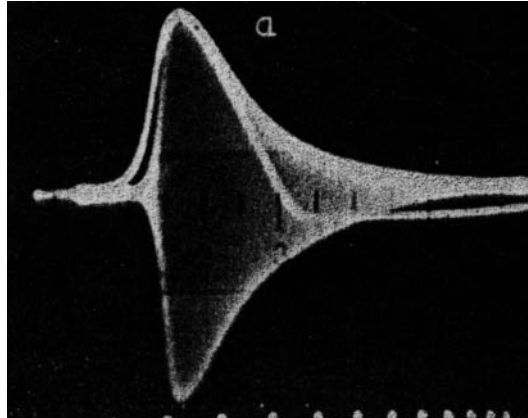


Figure 7-9: Conductance increase during excitation of the squid giant axon. The action potential is the first curve to rise from the baseline, peaks in about 1 ms and returns to below the baseline in just over 3 ms. The bottom line of pips are 1 ms marks. The conductance at each moment is the height difference between the top and bottom of the broad band of the white signal, which starts a half millisecond after the action potential, rises to a peak coincident with the action potential peak in just over 1 ms and returns to baseline in about 8 ms. (From Cole and Curtis, 1939, with permission from *J. Gen. Physiol.*)

exception of studies on giant cells, until the patch clamp techniques of Neher and Sakmann were invented in 1980. (Sakmann and Neher, 1995, give a review.)

### 7-6.2. The Hodgkin-Huxley nerve action potential

The equivalent circuit shown in Fig. 7-2 depicts only one current carrier. The currents through the capacitor and the resistor sum to zero:

$$C_m \frac{dV}{dt} + I_{\text{ion}}(V, t) = 0. \quad (7-65)$$

Given that there are two major current carriers (anticipating what Hodgkin and Huxley discovered) and some smaller leak currents, this translates to

$$C_m \frac{dV}{dt} = -g_{\text{Na}}(V - V_{\text{Na}}) - g_{\text{K}}(V - V_{\text{K}}) - g_{\text{L}}(V - V_{\text{L}}) + I_{\text{app}}, \quad (7-66)$$

where  $I_{\text{app}}$  is an applied current stimulus, and the subscripts Na, K and L represent the two cation currents and a general catchall leak current (Cl, Ca, etc.). The equivalent circuit is now revised, as shown in Figure 7-10, to account for three conductances.

By considering the conductance parameters, the  $g$ 's, to be time- and voltage-dependent, and the  $V$ 's to change over time, Eq. 7-66 allows for changes in the magnitude of conductances and driving forces over time; it assumes that the current flux is linearly proportional to the driving force at each specific value of  $g$ , and that the driving force is the electrochemical potential difference for each ion across the membrane. This is reasonably correct for small local perturbations induced by small applied currents,  $I_{\text{app}}$ , but deviates from the data when the shift of

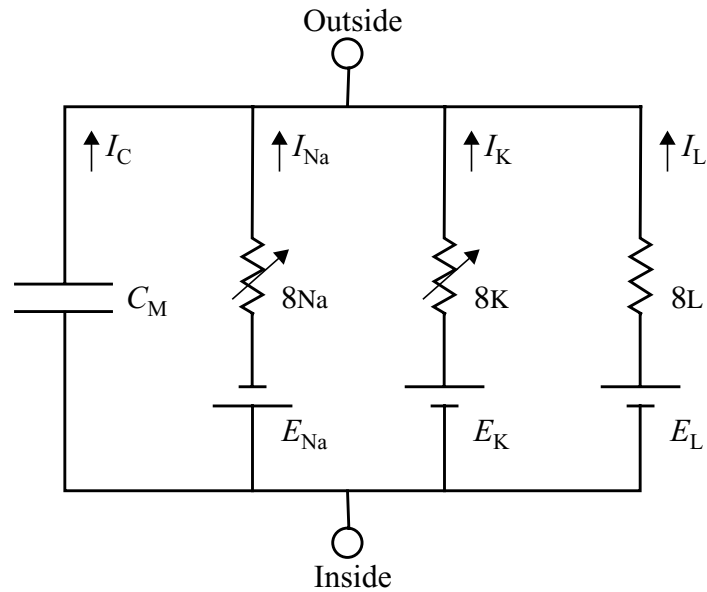


Figure 7-10: Circuit diagram for the Hodgkin-Huxley axon. Note that the voltages of the three “batteries” have sidedness dependent upon the charge gradients. (Redrawn from Hodgkin and Huxley, 1952e.)

voltage is more than several millivolts. An obvious question occurs: “Why are the currents not expressed in terms of the constant field assumption?” We return to this later, after examining the H-H experiments.

## 7-6.3. The voltage clamp methods for measuring transmembrane currents

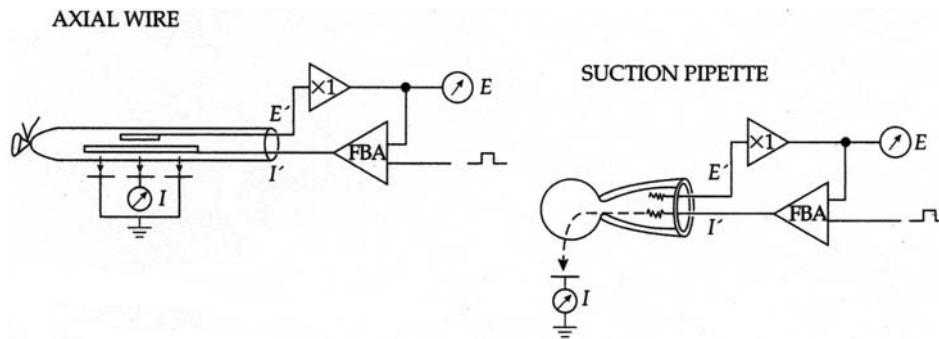


Figure 7-11: Voltage clamp methods for measuring transmembrane currents in excitable cells. The feedback amplifier, FBA, has inputs from the observed intracellular potential, and from signal generators providing the desired intracellular potential. The FBA output current, which is that which crosses the cell membrane, drives the intracellular voltage to match the desired voltage. Since this current must use the available ions and must flow through the membrane channels, it equals the total of the transmembrane currents. Dissection of the various ionic contributors to the current requires using a variety of different clamp step protocols, external solution concentrations, and channel blocking agents. (From Hille, 2001, with permission.)

The perceptiveness of Hodgkin and Huxley was in comprehending the complex relationships between their observations using the voltage clamp technique (Fig. 7-11) and a reasonable physical explanation. A key breakthrough was the decision to test the hypothesis that the potassium and sodium contributions of the currents were independent of each other. They did two types of experiments which demonstrated the sense of their notion. The first was to perform voltage clamp protocols to make voltage steps of a set of magnitudes and to record these and the current tails (the decay of current versus time from the steady-state current response back to the original baseline), and then to quickly repeat the sequence after removing the sodium from the external bathing solutions. The difference between the two sets of measured currents, at each clamp level, must be due to the  $\text{Na}^+$  current; the current time course after Na removal must be due to  $\text{K}^+$  current, as is shown in Fig. 7-12. Hodgkin and Huxley affirmed this later using the Na channel blocker tetrodotoxin, which is highly selective to that channel and can block it completely, and does not affect the K channel currents.

A key to the kinetics was to examine the tail current, the current that decays more or less exponentially on returning the clamp potential to the resting membrane potential or to some other level below or above the level of the depolarizing clamp step after the currents are activated. Fig. 7-13 shows that when a depolarizing clamp step is maintained for less than a millisecond, the dashed line in the upper panel returning to  $-65$  mV after about 0.6 ms, the tail current decays rapidly. The middle panel shows that the channel conductances were dominated by the Na channel opening at this early time. In contrast, when the return clamp step is taken later, at 6 ms, the tail current decay time is much longer, and since there was no apparent  $\text{Na}^+$  current at this late time, that decay is attributed to the diminution of the  $\text{K}^+$  current. From this experiment alone it may be tempting to believe that the potassium currents at all potentials might have much slower

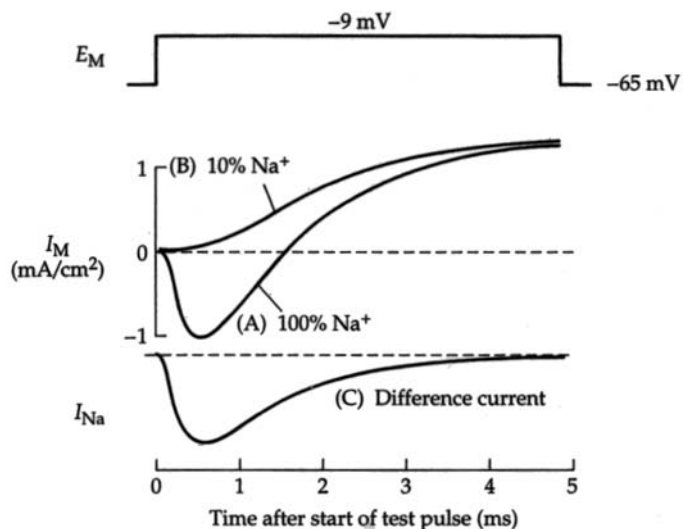


Figure 7-12: Determining the sodium current,  $I_{Na}$ , by difference. The difference current, panel C, is the difference between the two currents shown in panel B, and is due to a 90% reduction in  $[Na]_o$ . The estimated total  $I_{Na}$  is therefore 10/9 times this difference current. (From Hille, 2001, with permission.)

time constants than does the Na current, but this is not true, as is revealed by closer examination of the details.

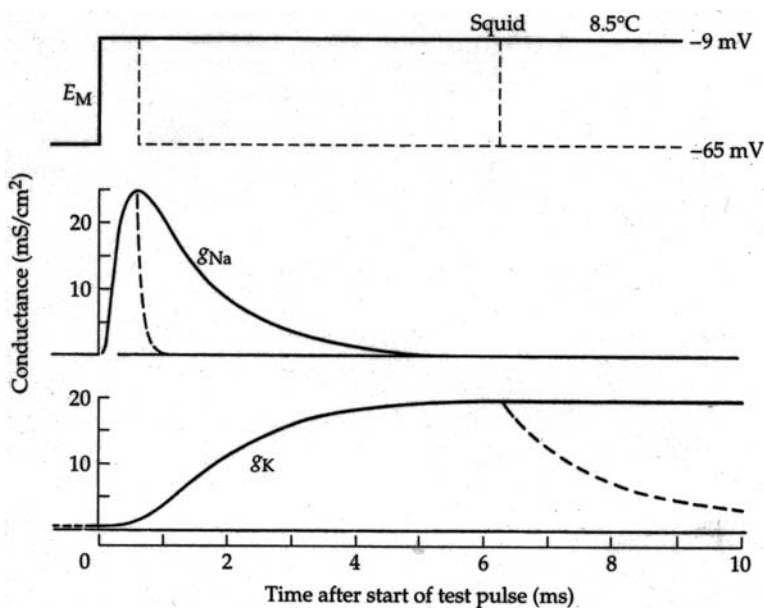


Figure 7-13: Short and long clamp steps in squid axon. The tail currents are the responses to the return of the clamp voltage to the baseline, the dashed lines of the upper panel. The Na tail current, the dashed line of the middle panel, is short. The K tail current last a few milliseconds.

Let's start with the equations for the  $g_{\text{Na}}$  and  $g_{\text{K}}$  in Eq. 7-66 ( $g_{\text{L}}$  is a constant). These conductances are functions of both voltage,  $E_{\text{m}}$ , and time; the changes in protein conformational state are induced by changes in voltage but take some time to occur. The equations are

$$g_{\text{Na}} = \bar{g}_{\text{Na}} m^3 h, \quad \text{and} \quad (7-67)$$

$$g_{\text{K}} = \bar{g}_{\text{K}} n^4, \quad (7-68)$$

where the time and voltage dependence of  $m$ ,  $h$  and  $n$  are given by empirical equations which capture the response times observed experimentally over a range of voltages. For example, for  $n$ ,

$$\frac{dn}{dt} = \alpha_n(1 - n) - \beta_n n = \frac{1}{\tau_n}(n_\infty - n), \quad (7-69)$$

the solution of which illustrates that this is an exponential relaxation from any initial state  $n_0$  at a voltage particular to the new state at the new voltage:

$$n(t) = n_\infty - (n_\infty - n_0) \exp(-t/\tau_n), \quad (7-70)$$

where  $n_\infty = \alpha_n/(\alpha_n + \beta_n)$  and  $\tau_n = 1/(\alpha_n + \beta_n)$ .

The equations for  $m$  and  $h$  are analogous. The voltage and time dependence of a conductance variable are combined in the descriptions of  $\alpha$  and  $\beta$ . Their description requires numerical values to be taken from the experimental data fitted by the model. Hodgkin and Huxley considered the resting potential to be at 0 mV, and depolarization was positive from there. We use modern current convention with the outside voltage zero and the inside negative, and also shift to mammalian concentrations: using the conductances they report gives us

$$\alpha_m = 0.1 \frac{V + 50}{1 - \exp\left(\frac{V + 50}{10}\right)}, \quad (7-71a)$$

$$\beta_m = 4 \exp\left(-\frac{(V + 75)}{18}\right), \quad (7-71b)$$

$$\alpha_h = 0.07 \exp\left(-\frac{(V + 75)}{20}\right), \quad (7-71c)$$

$$\beta_h = \frac{1}{\exp\left(-\frac{(V + 45)}{10}\right) + 1}, \quad (7-71d)$$

$$\alpha_n = 0.01 \frac{V + 65}{1 - \exp\left(\frac{-V - 65}{10}\right)}, \quad (7-71e)$$

$$\beta_n = 0.125 \exp(-(V + 75)/80), \text{ and in general,} \quad (7-71f)$$

$$\tau_v = \frac{1}{\alpha_v + \beta_v}, \text{ and } v_\infty = \frac{\alpha_v}{\alpha_v + \beta_v}. \quad (7-71g)$$

All  $V$ 's are in mV, current densities are in  $\mu\text{A}/\text{cm}^2$ , conductances are in  $\text{mS}/\text{cm}^2$ , and the time constants,  $\tau$ , and the  $\alpha$ 's and  $\beta$ 's are in ms. The maximum conductances for the three variables were  $\bar{g}_{\text{Na}} = 120$ ,  $\bar{g}_{\text{K}} = 36$  and  $\bar{g}_{\text{L}} = 0.3$ , all in  $\text{mS}/\text{cm}^2$ . With this transformed voltage reference to zero voltage outside, with  $\text{Na}_o = 143$ ,  $\text{Na}_i =$  the potentials were set at  $V_{\text{Na}} = +64.6$  mV,  $V_{\text{K}} = -88.6$  mV, and  $V_{\text{L}} = -60$  mV. The steady-state values of the conductance variables and their time constants are shown as function of voltage in Fig. 7-14.

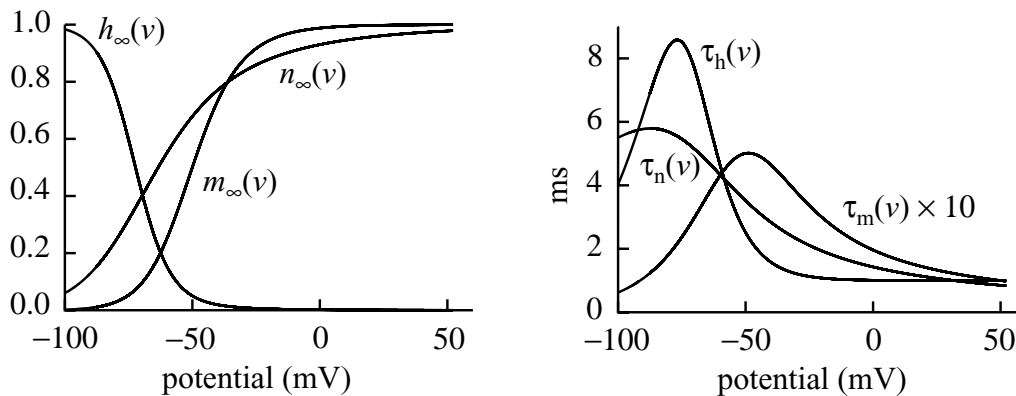


Figure 7-14: Steady-state functions for conductance variables, *left panel*, and for time constants, *right panel*, for the H-H-type nerve axon potential, plotted on the modern conventional voltage scale of zero potential outside and using mammalian concentrations. Note that  $\tau_m$  is scaled up ten-fold.

With these parameter values, the nerve action potential looks like that in Fig. 7-15. The actual code is given in Table 7-4 for the situation with a constant current input.

#### 7-6.4. Functional behavior of the nerve axon action potential

Giving a strong depolarizing stimulus to the axon at its resting potential guarantees that it will fire, that is, develop a regenerative action potential. It is “regenerative” because the more the depolarization, the more the Na channel’s  $m$  conductance variable increases. The word “regeneratively” indicates, in essence, positive feedback: more conductance  $\rightarrow$  more inward current  $\rightarrow$  more depolarization. Thus, in the upper panel of Fig. 7-15, the upslope  $dV/dt$  steepens as  $m^3$  increases, then becomes less steep as  $h$  decreases and the  $\text{K}^+$  current increases. The potential does not rise all the way to the sodium reversal potential,  $E_{\text{Na}}$ , because  $I_{\text{K}}$  is opposing  $I_{\text{Na}}$  and as  $I_{\text{Na}}$  diminishes  $I_{\text{K}}$  becomes dominant and drives the membrane potential back toward the resting

**Table 7-4: Hodgkin-Huxley model**

```

// Hodgkin-Huxley Model: (J. Physiol. 117:500-544, 1952)
// modified to use V as intracellular potential relative to extracellular space
// This description uses a constant current input Iext.
JSim v1.1 import nsrunit; unit msec = 0.001 sec; unit conversion on;
math hh { realDomain t msec; t.min=0; t.max=58.55; t.delta=0.05; // time
  private real Vu = 1 mV; // non-dimensionalizing V by V/Vu
  private real msm1 = 1 msec^(-1); // to balance units to tau
//PARAMETERS
real Nao = 143 mM, Nai = 12 mM, VNa = - (60 mV)*log(Nai/Nao),
  Ko = 5 mM, Ki = 150 mM, VK = - (60 mV)*log(Ki/Ko), VL = - 60 mV,
  Iext = 6e-3 mA/cm^2, Cm = 1 uF/cm^2,
  gbNa = 120 mS/cm^2, gbK = 36 mS/cm^2, gL = 0.3 mS/cm^2;
//VARIABLES defined as functions of time
real V(t) mV, m(t), h(t), n(t), taum(t) msec, minf(t), tauh(t) msec, hinf(t), taun(t) msec, ninf(t);

/*INITIAL CONDITIONS*/ when(t=t.min) {V = - 81.5; m = 0.023; h = 0.319; n = 0.531;}

//ALGEBRA for time constants and steady state functions for gating variables
taum=1/(msm1*(0.1*(V/Vu+50)/(1-exp(-(V/Vu+50)/10))+4*exp(-(V/Vu+75)/18)));
minf=(0.1*msm1*(V/Vu+50)/(1-exp(-(V/Vu+50)/10)))*taum;
tauh=1/(msm1*(0.07*exp(-(V/Vu+75)/20)+(1/(1+exp(-(V/Vu+45)/10))));
hinf=0.07*msm1*exp(-(V/Vu+75)/20)*tauh;
taun=1/(msm1*(0.01*(V/Vu+65)/(1-exp(-(V/Vu+65)/10))+0.125*exp(-(V/Vu+75)/80)));
ninf=(0.01*msm1*(V/Vu+65)/(1-exp(-(V/Vu+65)/10)))*taun;

//ODEs:
V:t=(-gbNa*m^3*h*(V-VNa)-gbK*(V-VK)*n^4-gL*(V-VL)+Iext)/Cm;
m:t=-(m-minf)/taum;
h:t=-(h-hinf)/tauh;
n:t=-(n-ninf)/taun;
}

```

potential. (The process thus degrades both the Na and K gradients a little bit, requiring restoration by the NaK ATPase.)

The peak values of  $dV_m/dt$  in Fig. 7-15 provide a measure of peak current flow. The current is  $C_m \cdot dV_m/dt$ , so with  $C_m = 1 \mu\text{F}/\text{cm}^2$  membrane area and  $dV_m/dt = 40 \text{ mV}/\text{ms}$ , using the Terminology of Chapter 1 for the units and assuming that the current is maintained for 1 ms (about the amount of time needed for the action potential to reach its peak), the charge transferred is

$$\begin{aligned}
 \text{Charges transferred} &= \int_0^{1 \text{ ms}} C_m \cdot \frac{dV}{dt} dt = \frac{1 \mu\text{F}}{\text{cm}^2} \cdot 40 \frac{\text{mV}}{\text{ms}} \cdot 1 \text{ ms} = 2.5 \cdot 10^{11} \frac{\text{charges}}{\text{cm}^2} \\
 &= 15 \cdot 10^6 \text{ charges / cell (for a cell with } r = 8 \mu\text{m, } L = 120 \mu\text{m)},
 \end{aligned}$$

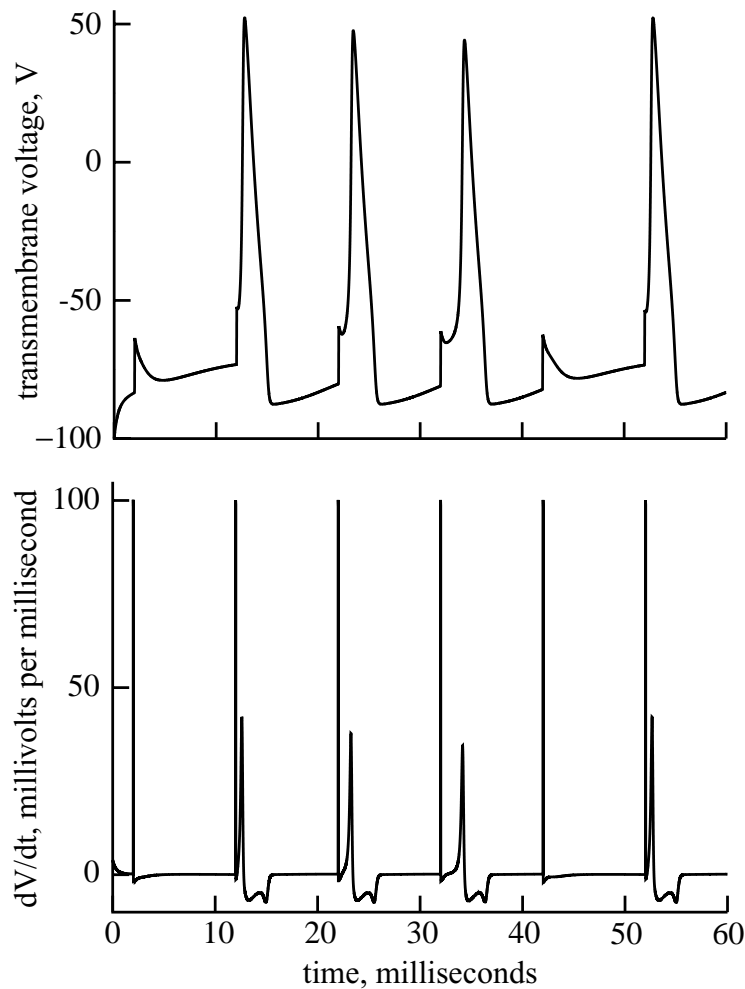


Figure 7-15: Hodgkin-Huxley nerve action potential. Normal action potential evoked with a very minimal stimulus,  $6.3 \mu\text{A}/\text{cm}^2$ , 0.02 ms pulse stimulus every 10 ms. The initial  $V_m$  was set to  $-100\text{mV}$ . The rate of rise of  $dV_m/dt$  is shown in the bottom panel. The stimuli force  $dV_m/dt$  to reach  $100 \text{ mV}/\text{ms}$  momentarily. For the initial stimulus in the series the charge transferred was not enough to trigger a regenerative depolarization. With a second stimulus an action potential was evoked, with a peak depolarization rate of about  $40 \text{ mV}/\text{ms}$  (with a peak influx rate of  $2500 \text{ ions}/\text{ms}$  per square micron surface area). The regenerative depolarizing current lasts longer than the very short stimulus pulse. The peak rate of rise of the third action potential (following the fourth stimulus at 32 ms) is  $34.5 \text{ mV}/\text{ms}$ , reduced compared to the other that fired an AP, but this one is over 2 ms after the stimulus and the rate of depolarization is due solely to the flux through the Na channel minus some retarding outward current due to increasing K channel conductance. The fourth is even more delayed, has barely started its regenerative depolarization, and has a lower maximal  $dV_m/dt$ . The fifth of these minimal stimuli failed to bring  $V_m$  to the stage of regenerative depolarization, and merely decayed, like the first response.

$$= 2500 \text{ charges / square } \mu\text{m surface area.}$$

From this, if one knows the conductance per channel, one could estimate the numbers of channels per cell

Because the time required for complete inactivation of  $h$  is longer than the action potential remains above  $-20$  mV,  $h$  is never completely reduced to zero. Likewise, even though  $m$  activates rapidly, it does not reach 1.0 during a normal action potential. Consequently it is understandable that because of the incompleteness of the return to the resting conditions, the shape of the action potential is somewhat dependent on the rate of firing. Such rate-dependent changes in AP form are very much more evident in cardiac APs than in nerve.

Changes in the external ionic milieu affect the sensitivity to a depolarizing pulse. Raising external potassium to 20 mM depolarizes the membrane. While this might at first blush make one think that the membrane potential, now reduced to  $-54$  mV and close to the  $-60$  mV threshold for the Na channel activation, would make the cell highly sensitive to mild depolarizing spikes, the effect is quite the opposite. The reason is that the  $h$  variable for Na conductance is now much less than unity, and the cell is almost unexcitable. Exploring behavior using the computer model is a valuable tool for gaining insight into the physical and mathematical aspects of the system resulting in specific behavior. The program in Table 7-4 can be run as it is under JSim, or downloaded from [nsr.bioeng.washington.edu](http://nsr.bioeng.washington.edu).

### 7-6.5. Cardiac and other action potentials

The Hodgkin-Huxley nerve action potential provides the basic Na and K currents for the action potentials of other cells. It seems likely that the phylogenetic development of these channels was relatively early and has been passed down from rather primitive organisms, like the nematode worm *Caenorhabditis elegans*, all the way to mammals. While the parameter values differ somewhat from species to species the basic form of the conductance equations remains constant. What is even more remarkable in the insight of Hodgkin and Huxley is the close analogy between the kinetic mechanism they surmised might operate for a four-component channel and the recently elucidated four-module form of the protein.

Nerves and skeletal muscle action potentials in frogs and mammals have a small calcium current in addition to  $I_{\text{Na}}$  and  $I_{\text{K}}$ . In cardiac muscle  $I_{\text{Ca}}$  is large and causes a prolonged plateau phase of depolarization, which in turn prolongs the action potential a hundred-fold compared to a nerve. The early cardiac AP model of Noble (1962) attempted to explain the long plateau phase of the AP by a prolongation of the opening of the Na channel. The observations of Beeler and Reuter (1970) and of Bassingthwaite and Reuter (1972) clarified the role of an inward calcium current which provided a better explanation. The calcium current was found to have time and voltage dependencies analogous to those of the Na channel, but was slower to activate and to inactivate. Its conductance was moderately high, so the inward  $I_{\text{Ca}}$  was strong enough to offset the outward  $I_{\text{K}}$  for over 200 msec, maintaining the plateau phase of the AP near 0 mV before  $I_{\text{K}}$  took over to bring about repolarization.

**Problem:** Given the ionic flux of 2500 ions/ms (legend of Fig. 7-15) and single channel maximum conductance equal to those of Fig. 7-5, what is the surface density of channels? (Answer: Single channel current = 0.8 pA =  $0.8 \times 10^{-12}$  Coulombs/sec; 1 Coulomb =  $6.243 \times 10^{18}$  elementary charges ( $z = 1$ ), giving 0.8 pA = 5000 charges/ms, and a min. density of 0.5 chan/ $\mu^2$ .)

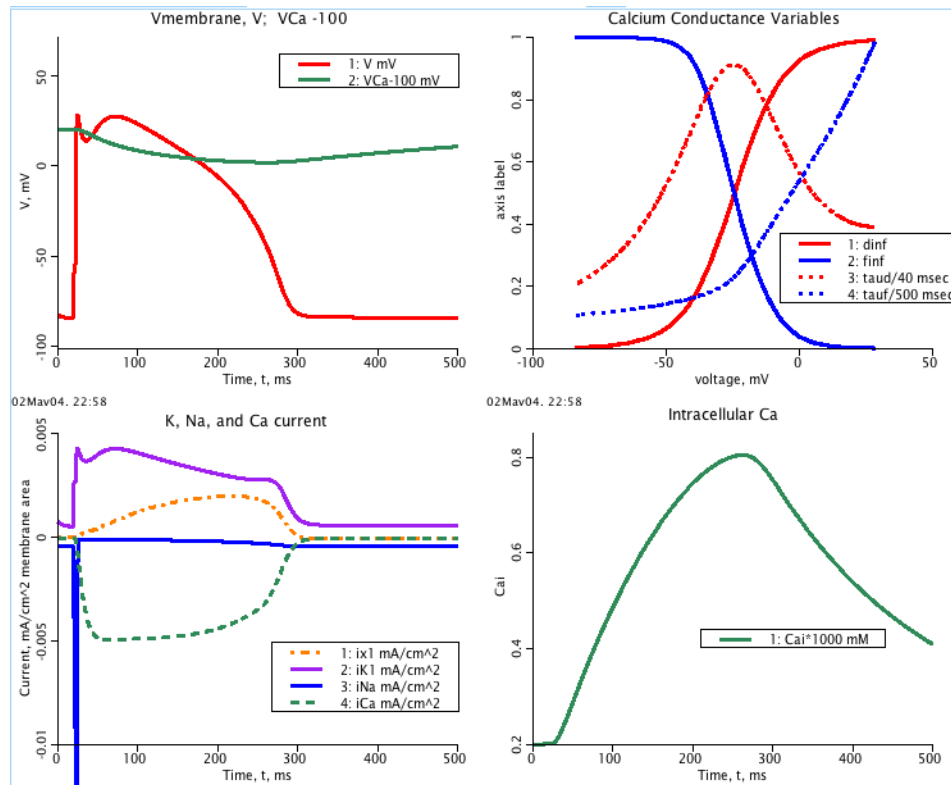


Figure 7-16: Beeler-Reuter cardiac action potential model. *Upper left*: Standard action potential (red) and  $E_{Ca} - 100$  mV (green, the Ca Nernst potential  $- 100$  mV for display). *Lower left*: The four currents,  $i_{K1}$  (purple),  $i_{Na}$  (blue) which goes off scale,  $i_{Ca}$  (dashed green), and  $i_{x1}$  (dashed orange). *Right upper*: Ca variables,  $d$  and  $f$  and their time constants. *Right lower*: Intracellular Ca,  $[Ca]_i$ , during the action potential.

#### 7-6.5.1. The Beeler-Reuter cardiac ventricular action potential:

The Beeler-Reuter (1977) model is a four-current model in which there is a voltage-dependent  $K^+$  current,  $I_{K1}$ , and time- and voltage-dependent currents, in the style of the Hodgkin-Huxley model, for inward currents  $I_{Na}$ ,  $I_{Ca}$ , and an outward current  $I_{x1}$ , which is mainly potassium. This model described the action potential rather well in terms of these currents, but parameters that really incorporate the effects of currents, namely those that were unknown at the time or considered to be very small, were not considered. Thus, while the model gives remarkably faithful descriptions of the experimental voltage clamp data, it is inevitably found wanting when the physiological conditions deviate widely from the laboratory conditions. For example there is no consideration given directly to the modification of the potassium conductances that occurs when external calcium concentration is changed.

The action potential and other variables are shown in Fig. 7-16. The long action potential of about 300 ms duration in the left upper panel is due to the prolonged inward currents shown in the left lower panel, mainly due to  $I_{Ca}$ , but with a small continuing Na contribution to  $I_{Na}$  due to the Na leak current controlled by a constant conductance  $g_{NaC}$ . Repolarization occurs when the combined outward currents,  $I_{K1} + I_{x1}$ , exceed  $I_{Ca} + I_{Na}$  after about 250 ms.

The code for the Beeler-Reuter model is given in Table 7-5; the ODE's are written in very compact form but follow the same definitions as for the HH model (Eq. 7-71f). For the calcium

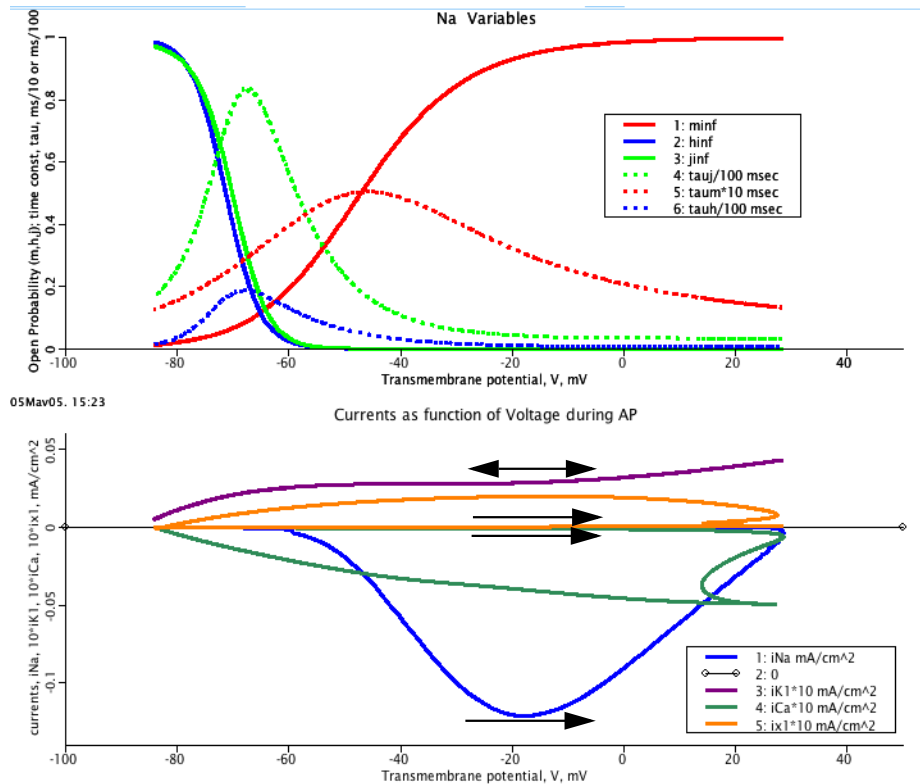


Figure 7-17: The  $i_{Na}$  conductance variables, time constants and currents in the BR model. *Upper panel*: Solid lines are  $m_{\infty}$  (red),  $h_{\infty}$  (blue), and  $j_{\infty}$  (green), while the dashed lines are their voltage-dependent time constants  $\tau_m(V)$ ,  $\tau_h(V)$ , and  $\tau_j(V)$ . *Lower panel*: Phase plane plots of currents versus transmembrane voltage  $V$  during the action potential. The  $i_K$ , having no time-dependence, shows no hysteresis. Depolarization phase: rightward arrows.

current there is an activation variable  $d(t, V)$ , which at a constant voltage takes on a value  $d_{\infty}(V)$ , and an inactivation variable  $f(t, V)$ , the steady-state value of which is  $f_{\infty}(V)$ , shown in the right upper panel of Fig. 7-16 along with the voltage-dependent time constants,  $\tau_d(V)$  and  $\tau_f(V)$ . Note that the time constants are very different,  $\tau_d(V)$  being divided by 40 for display and  $\tau_f(V)$  being divided by 500, so it is 12.5 times slower than  $\tau_d(V)$ . The steady-state shape of  $d_{\infty}$  is close to that of  $m_{\infty}$ , but with 50% activation at  $-25$  mV. It is not cubed. The inactivation variable  $f_{\infty}$  has its 50% activation at about the same voltage as does  $d$ ; the consequence of this is that there is, in the steady state, a window or “notch” centered at  $-25$  mV where the calcium channel remains open. This has a major influence on the form of the action potential, greatly prolonging it by virtue of the inward  $Ca^{2+}$  current keeping the membrane potential near zero, and creating the long plateau phase of the cardiac action potential. The prolonged inward current leads to an increase in intracellular  $Ca_i$ , right lower panel of Fig. 7-16, which is sufficient to induce contraction. Even so, this is not a model suitable for use in understanding excitation-contraction coupling because in reality a large fraction of the  $Ca^{2+}$  which binds to troponin does not come from the extracellular space but from triggered release from storage in the sarcoplasmic reticulum. In skeletal muscle, the action potential is much shorter, the  $Ca^{2+}$  influx much less, so that almost all of the contraction-stimulating calcium comes from the SR release. A further problem with this model is

**Table 7-5: JSim code for Beeler Reuter cardiac action potential**

```

math brjbb { realDomain t msec; t.min=0; t.max=650; t.delta=0.1; // time
//modified slightly by JBB from Beeler Reuter J Physiol 1977 to use Nernst potentials, but does not
// include any dependence of the K currents, iK1 and ix1, on [Ca]o, as BR did not include it.
  private real Vu = 1 mV, msm1 = 1 msec^(-1); // to balance units, V/Vu & in the tau's
//PARAMETERS
real Nao=143 mM, Nai=12 mM, VNa=-(60 mV)*log(Nai/Nao), gNaC = 0.003 mS/cm^2,
  Ko=5 mM, Ki=150 mM, VK=-(60 mV)*log(Ki/Ko), Vrest = VK +0.015*VNa,
  Cao=2 mM, Cai0=2e-4 mM, tauCa = 150 msec,
  Caconst= 1e-4 mM*msec^(-1)*cm^2/mA, /*=molar flux per volume per current*/
  gbNa=4 mS/cm^2, gbCa =0.09 mS/cm^2,Cm=1 uF/cm^2, clamp_flag = 0, pulsamp=0. 05;
/*VARIABLES*/ real V(t) mV, VV(t) mV, VCa(t) mV, Iion(t) mA/cm^2, iNa(t) mA/cm^2,
  m(t),h(t),j(t),taum(t) msec, minf(t),tauh(t) msec,hinf(t),tauj(t) msec,jinf (t),
  x1(t),taux1(t) msec,x1inf(t), ix1(t) mA/cm^2, ibx1(t) mA/cm^2, iK1(t) mA/cm^2,
  iCa(t) mA/cm^2, Cai(t) mM, d(t),f(t),taud(t) msec,dinf(t),tauf(t) msec,finf (t);
extern real Iext(t) mA/cm^2, Vclamp(t) mV;
/*INIT COND*/ when (t=t.min) { m=0.0104;h=0.989;j=0.976;x1=0.0054; d=0. 003;
  f=0.9999; Cai=Cai0; VV=if(clamp_flag=0) Vrest else Vclamp ; }
//ALGEBRA for time constants and steady state functions for gating variables
ibx1 = (0.0008 mA/cm^2)*(exp(0.04*(V/Vu+77))-1)/exp(0.04*(V/Vu+35));
taux1=1/(msm1*((0.0005*exp(0.083*(V/Vu+50)))/(1+exp(0.057*(V/Vu+50)))
  +0.0013*exp(-0.06*(V/Vu+20)))/(exp(-0.04*(V/Vu+20))+1));
x1inf=taux1*msm1*(0.0005*exp(0.083*(V/Vu+50)))/(1+exp(0.057*(V/Vu+50)));
taum=1/(msm1*((-1*(V/Vu+47))/(exp(-0.1*(V/Vu+47))-1)+40*exp(-0.056*(V/Vu+72))));
minf=taum*msm1*(-1*(V/Vu+47))/(exp(-0.1*(V/Vu+47))-1);
tauh=1/(msm1*(0.126*exp(-0.25*(V/Vu+77)))+(1.7/(1+exp(-0.082*(V/Vu+22.5)))));
hinf=tauh*msm1*0.126*exp(-0.25*(V/Vu+77));
tauj=1/(msm1*((0.055*exp(-0.25*(V/Vu+78)))/(1+exp(-0.2*(V/Vu+78)))
  +0.3/(exp(-0.1*(V/Vu+32))+1));
jinf=tauj*msm1*(0.055*exp(-0.25*(V/Vu+78)))/(1+exp(-0.2*(V/Vu+78)));
taud=1/(msm1*((0.095*exp(-0.01*(V/Vu-5)))/(1+exp(-0.072*(V/Vu-5)))
  +0.07*exp(-0.017*(V/Vu+44))/(exp(0.05*(V/Vu+44))+1));
dinf=taud*msm1*(0.095*exp(-0.01*(V/Vu-5)))/(1+exp(-0.072*(V/Vu-5)));
tauf=1/(msm1*((0.012*exp(-0.008*(V/Vu+28)))/(1+exp(0.15*(V/Vu+28)))
  +0.0065*exp(-0.02*(V/Vu+30))/(exp(-0.2*(V/Vu+30))+1));
finf=tauf*msm1*(0.012*exp(-0.008*(V/Vu+28)))/(1+exp(0.15*(V/Vu+28)));
iNa = (gbNa*m^3*h*j +gNaC)*(V -VNa);
iK1 = (0.00035 mA/cm^2)*(4*(exp(0.04*(V/Vu+85))-1)/(exp(0.08*(V/Vu+53))
  +exp(0.04*(V/Vu+53))) +0.2*(V/Vu+23)/(1-exp(-0.04*(V/Vu+23))));
ix1 = ibx1*x1;
iCa = gbCa*d*f*(V-VCa); VCa =-(30 mV)*log(Cai/Cao);
Iion = iNa+iK1 +ix1 +iCa;

/*ODEs*/ VV:t = if (clamp_flag=0) - (Iion-Iext*pulsamp)/Cm else (0 mV/s);
  V = if (clamp_flag=0) VV else Vclamp;
Cai:t = -iCa*Caconst - (Cai-Cai0)/tauCa;
m:t=(minf-m)/taum; h:t=(hinf-h)/tauh; j:t=(jinf-j)/tauj;
x1:t=(x1inf-x1)/taux1;
d:t=(dinf-d)/taud; f:t=(finf-f)/tauf;
}

```

its basic assumption that the intracellular concentrations in the cytosol are uniform; Bassingthwaite and Reuter (1972) observed considerably larger shifts in the apparent  $E_{Ca}$  than are found with the BR model even though the  $Ca^{2+}$  current is too large. The difference is explicable by including a small subspace at the sites of the Ca channels, namely at the apposition regions between T-tubular sarcolemma and the cisternae of the SR (sarcoplasmic reticulum);  $Ca^{2+}$  would transiently accumulate within this space before diffusing out into the cytosol.

The Na fluxes shown in Fig. 7-17 are taken from the HH expressions with little modification: the shapes of the  $m_{\infty}$  and  $h_{\infty}$  curves are rather similar to those in Fig. 7-14. There is one difference however, in that  $\tau_m(V)$  is 10 times shorter in the BR model than in the HH model. It seems that this might be a mistake since the authors intended them to be the same; in practice it makes little difference since even with a slower squid axon  $\tau_m(V)$  the upstroke of the action potential is not slowed noticeably, and the difference is less than the measurement error in the data. The current-voltage plots in the lower panel of Fig. 7-17 show that  $I_{Na}$  is activated rapidly and has a maximum current more than 20 times that of the others, which are all scaled up by a factor of 10 relative to  $I_{Na}$ .

Fig. 7-18 shows the time courses of the sodium and calcium conductance variables during

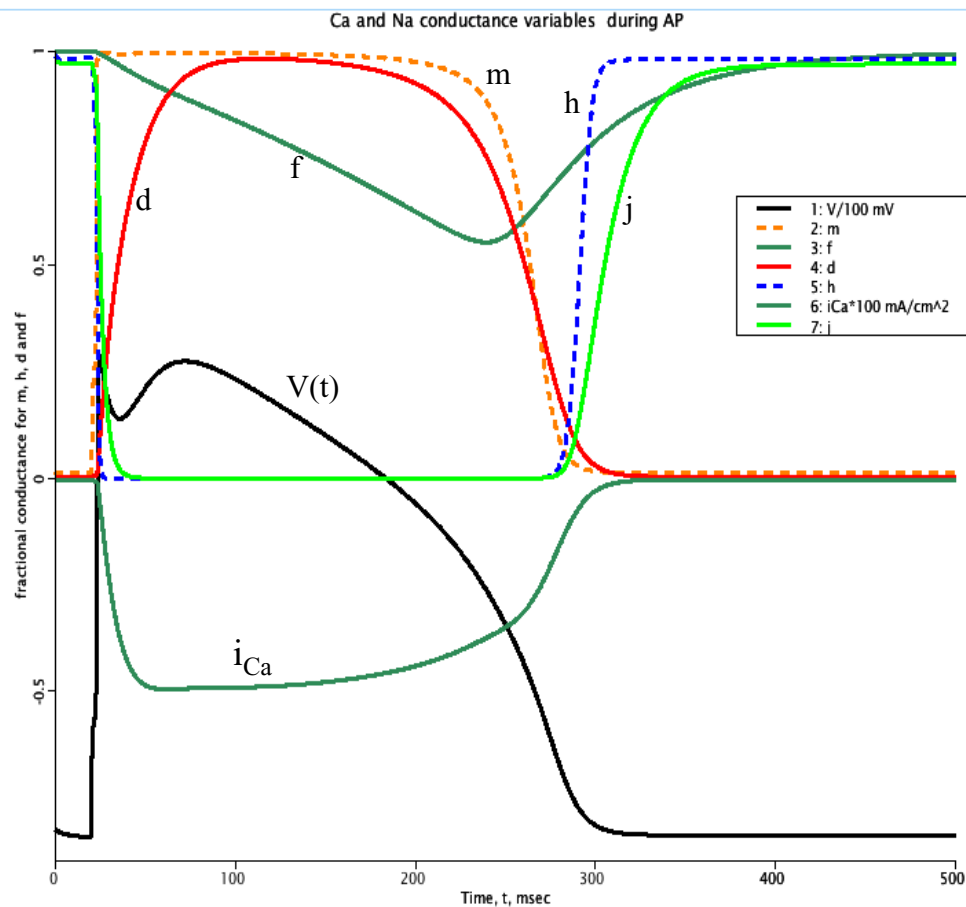


Figure 7-18: Time courses of Beeler-Reuter conductance variables during an action potential.

the progress of an action potential. The  $m(t, V)$  turns on quickly and  $h(t, V)$  turns off very soon, so the transient  $I_{Na}$  is complete in a few milliseconds. The  $Ca^{2+}$  activation variable  $d$  takes over 50 ms to reach its peak at just less than 1.0, while the variable  $f$  diminishes from 1.0 almost linearly though it is still at about 60% when repolarization occurs. The slow and incomplete inactivation allows the  $i_{Ca}$  to remain strong, and thereby prolongs the action potential more than in other tissues.

Fig. 7-19 shows the potassium conductances, i.e., those for  $I_{k1}$  and  $I_{x1}$ . The conductance variable  $x_1$  does not reach 0.4 during the action potential, so the product  $I_{bx1} * x_1$  remains low, and the current  $I_{x1} = I_{bx1} * x_1$  turns on slowly but ends up having a strong influence on inducing repolarization.

The BR model stands out as an easy model to work with, and represents the major features of the action potential. It is also simple, and not demanding computationally, so it can also be used in programs for the spatial spread of excitation. The Fitzhugh-Nagumo model (Fitzhugh, 1961; Nagumo et al., 1964) is simpler still, and is also in programs for the spatial spread of excitation, but is much farther from having a solid physiological basis.

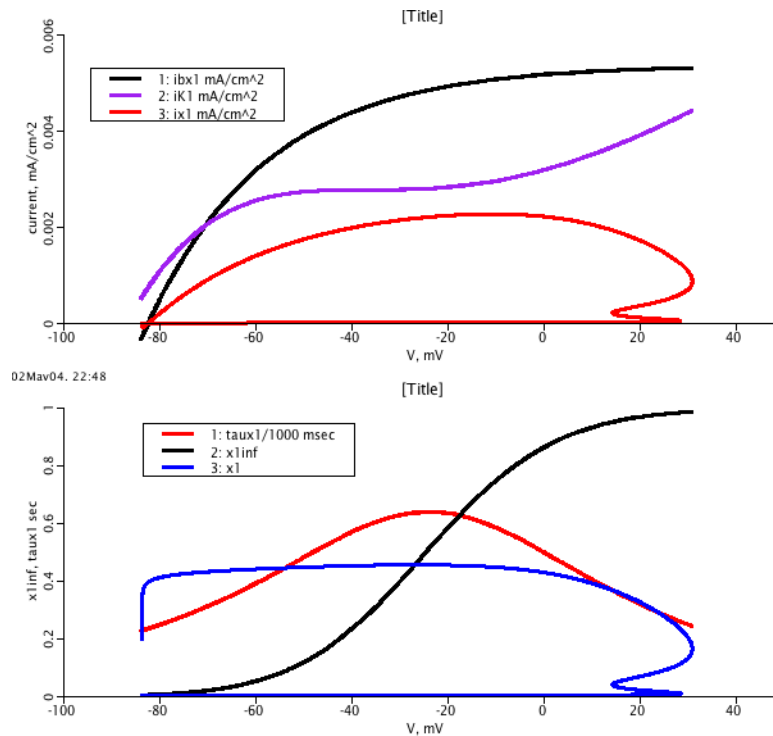


Figure 7-19: Potassium channel conductances. *Upper panel:* The potassium current  $i_{K1}$  (purple), the mixed, mostly  $K^+$ , current  $i_{x1}$  (red), and its maximal conductance variable  $i_{bx1}$  (black). *Lower panel:* The time constant for  $i_{x1}$ ,  $\tau_{x1}$  (red), divided by 1000 and peaking at 0.6 seconds at about  $V = -25$  mV, and its  $x_{1\infty}$  (black). The current  $i_{x1} = i_{bx1} * x_1$ , where  $x_1$  (blue) is the opening probability during the action potential.

#### 7-6.5.2. Other action potential models:

More advanced cardiac AP models have been developed since. A critical feature introduced into these is accounting for fluxes due to exchangers and the pumps. Cardiac ventricular action potential models have developed along three closely related tracks, each attempting to account in an integrative fashion for a wealth of experimental data on cardiac electrophysiology. The three closely related tracks are exemplified by (1) the model of Yoram Rudy and colleagues (Luo and Rudy, 1991, 1994a,b and about 10 subsequent papers), which includes ion pumps and exchangers and achieves overall ionic balance; (2) the model of Rai Winslow and colleagues (Jafri et al., 1998, 1999; Winslow et al., 1999; Greenstein et al., 2000) and (2a) more recently improved versions, particularly an independent one built upon the Winslow model by Michailova and McCulloch, 2001, that includes buffering of the calcium levels by MgATP as well as buffering by troponin C and calmodulin. These are strong on the electrophysiology but weak with regard to pumps and exchangers and do not provide long-term sodium balance; (3) the model of Noble's group in Oxford (Noble et al., 1998; Kohl et al., 1999, Sakmann et al., 2000) which gives excellent adherence to data from their own experiments and includes slightly different  $K^+$  currents than the other models as well as being better linked to the effects of  $H^+$  ion and metabolism.

**[\[Add JBAP model, with code in an Appendix or on web.\]](#)**

A current model, developed under JSim, will be made available on the web (at <http://nsr.bioeng.washington.edu, jbAP>) concurrently with this book's publication, and provides

ionic balance, buffering of calcium, phosphate balance, and energy balance, but at the cost of developing the ionic pumps to a new level and requiring more computer time. **[This section will be enlarged in the next revision.]**

## 7-7. Propagation of the action potential

### 7-7.1. The cable equations

The nerve is a leaky cable. It is composed of a long cylindrical membrane surrounding conductive cytoplasm, and is itself surrounded by a conductive milieu. The diameter is miniscule compared to the length, so a one-dimensional approximation works well: i.e., one can assume that the core has no radial concentration or potential gradients (Rall, 1977), the *core conductor assumption*. The circuit diagrams considered for the action potential now need to be augmented to account for the length of the nerve and therefore for the non-uniformity of the potential with position, as diagrammed in Fig. 7-20.

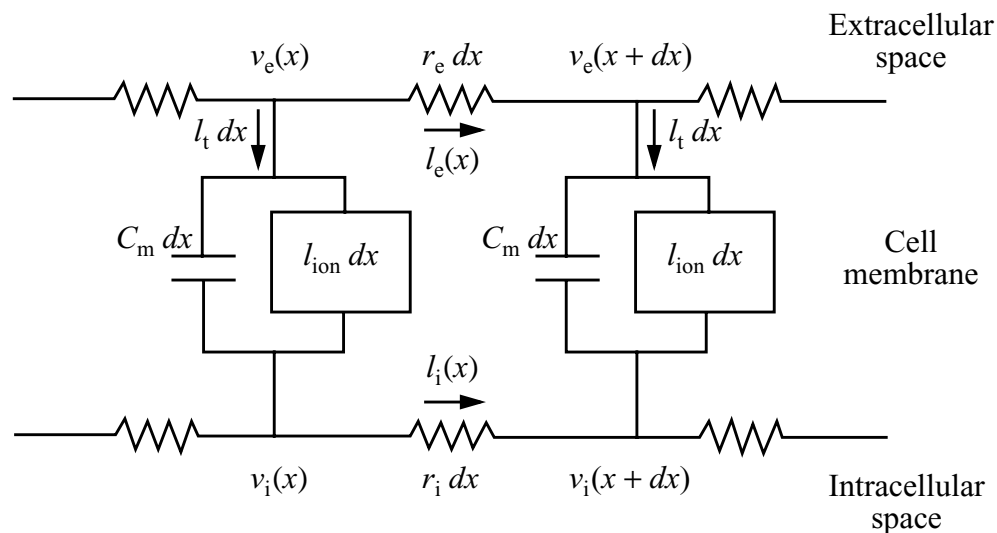


Figure 7-20: Circuit diagram for a one-dimensional cable representation of a nerve axon. The discretization of  $x$ ,  $x + dx$ ,  $x + 2dx$ , etc., defines discrete currents and potential gradients along  $x$  and for the propagation of the depolarization along the neuron. (Adapted from Fig. 8.2 of Keener and Sneyd, 1998.)

The figure shows a discretized version of a continuous system representing a one-dimensional cable. It provides a good model for propagation along an unmyelinated nerve. In myelinated nerves the sites of local transmembrane current flow are not everywhere along the membrane, but are only at distinct locations, the Nodes of Ranvier, semi-exposed parts of the axon between successive insulating Schwann cells. Cardiac cells have no insulating layer surrounding them but, unlike nerve cells, have extensive lateral as well as terminal gap junctional connections so that cell-to-cell conductance laterally is almost one-third of that axially. This means that cardiac cells really form a three-dimensional cable.

Weidmann (1952) found that the one-dimensional cable equation described the electrical spread in cardiac Purkinje fibre (the specialized conducting cells of the heart) as well as it did nerve conduction. Axial electrical conductivity is evident in all cells as electrotonic spread of

potential along a membrane; in excitable cells the electrotonic spread leads to regenerative depolarization which is the basis for excitatory propagation. The basic cable equation, assuming that extracellular resistance is small, is

$$i_m = \frac{1}{r_i} \cdot \frac{\partial^2 V_m}{\partial x^2} = \frac{V_m}{r_m} + C_m \cdot \frac{\partial V_m}{\partial t}, \quad (7-72)$$

where  $i_m$  is current flow across a 1 cm. length of cable;  $r_i$  is the longitudinal resistance of a unit length of cytosol inside the nerve,  $\Omega/\text{cm}$ ;  $V_m$  is  $V_m(x,t)$ , the transmembrane voltage, volts, and the difference between  $V_e$  and  $V_i$ ;  $r_m$  is the transmembrane resistance,  $\Omega \cdot \text{cm}$ , which is the transmembrane resistivity or resistance per unit membrane area,  $\Omega \cdot \text{cm}^2$ , divided by the perimeter of the fiber, cm;  $c_m$  is the membrane capacitance of about  $1 \mu\text{F}/\text{cm}$  length of cable. This expression omits consideration of the extracellular resistance  $r_e$ ,  $\Omega/\text{cm}$ , and is therefore applicable for a cable in a large-volume medium where the cross-sectional area is so large that  $r_e$  can be considered zero. Note that the units differ from those used in describing the action potential, which were all for a point on a membrane.

The derivation goes as follows, using the setting from Fig. 7-20:

$$V_i \cdot (x + \Delta x) - V_i \cdot (x) = -i_i(x)r_i\Delta x, \quad (7-73)$$

$$V_e \cdot (x + \Delta x) - V_e \cdot (x) = -i_e(x)r_e\Delta x, \quad (7-74)$$

where  $i_i$  and  $i_e$  are the intracellular and extracellular axial currents. The designation of the currents as having a negative sign when positive charges flow to a larger  $x$  is an accepted convention. The difference equations become differential equations as  $\Delta x \rightarrow 0$ :

$$i_i(x)r_i = \frac{\partial V_i}{\partial x}, \text{ and} \quad (7-75)$$

$$i_e(x)r_e = -\frac{\partial V_e}{\partial x}. \quad (7-76)$$

When the cross-sectional area of the external solution is large,  $r_e \rightarrow 0$ , then  $i_e$  is zero and  $V_m$  is the same as  $V_i$ , so Eq. 7-75 can be rewritten as

$$\frac{\partial V_m}{\partial x} = -i_i r_i. \quad (7-77)$$

The current  $-i_m$  lost across each unit length of membrane,  $\Delta x$ , reduces the longitudinal flow of cytosolic or core current at points farther along (higher  $x$ ), so

$$\frac{\partial i_i}{\partial x} = i_m. \quad (7-78)$$

Differentiating Eq. 7-77 and substituting Eq. 7-78 into the standard equation for transmembrane current at a point on the membrane, as for the action potential, we obtain the cable equation:

$$\frac{1}{r_i} \cdot \frac{\partial^2 V_m}{\partial x^2} = \frac{V_m}{r_m} + c_m \cdot \frac{\partial V_m}{\partial t}. \quad (7-79)$$

Analysis of cardiac and neural electrophysiological responses to current step at a point along the cable illustrated that the potential spread some distance to either side. In the steady state, the falloff in potential is exponential and the space constant is

$$\lambda_m = \sqrt{r_m / (r_i + r_o)} \text{ cm}, \quad (7-80)$$

and the time constant for the signal to approach the steady state is  $\tau_m = r_m c_m$ . The space constant is the distance for the peak potential at the site of the current electrode to fall to  $1/e$ , or 0.3678, of the peak potential. The time constant is the time for the potential to fall to  $1/e$  of its steady-state value when the current is turned off or, in general, for the change from one steady state to another to progress to  $1 - 1/e$  or 63% of the way to the new steady state. The cable equation can be rephrased to use these characteristic time and distance constants:

$$\lambda_m^2 \cdot \frac{\partial^2 V_m}{\partial x^2} + \tau_m \left( \frac{\partial V_m}{\partial t} + V_m \right) = 0. \quad (7-81)$$

Further treatment of this equation is given by Jack, Noble and Tsien (1975). At a point of steady current stimulation with current  $I_0$  the resultant voltage is given by Eq. 7-82, where the 2 in the denominator is due to the fact that the current flows off in two directions. (If the current stimulus is near an end of the “cable” the flow is almost unidirectional, so the 2 would become close to 1.0.),

$$V_0 = r_i I_0 \lambda_m / 2, \quad (7-82)$$

and the voltage as a function of distance is

$$V(x) = V_0 e^{-x/\lambda_m}. \quad (7-83)$$

If we define an input resistance  $R_{in}$  then

$$R_{in} = V_0 / I_0 = \sqrt{r_m r_i}.$$

A further translation into experimentally accessible terms considers these together with nerve surface area or cross-sectional area:

$$R_m = 2\pi a r_m, \quad (7-84)$$

$$R_i = \pi a^2 r_i, \quad \text{and} \quad (7-85)$$

$$C_m = c_m / 2\pi a, \quad (7-86)$$

where  $a$  is the radius,  $R_m$  is the resistance of 1 cm<sup>2</sup> of membrane with units  $\Omega/\text{cm}^2$ ,  $R_i$  is the intracellular longitudinal resistance  $\Omega/\text{cm}$ , and  $C_m$  is the capacitance of 1 cm<sup>2</sup> of membrane in  $F/\text{cm}^2$ . Although cardiac Purkinje fibers, strings of cells forming the conduction system of the heart, do not have the simple forms of cylindrical cable-like neurons, in fact these equations serve well for the description of passive properties, as demonstrated in Fig. 7-21 from Weidmann (1952).

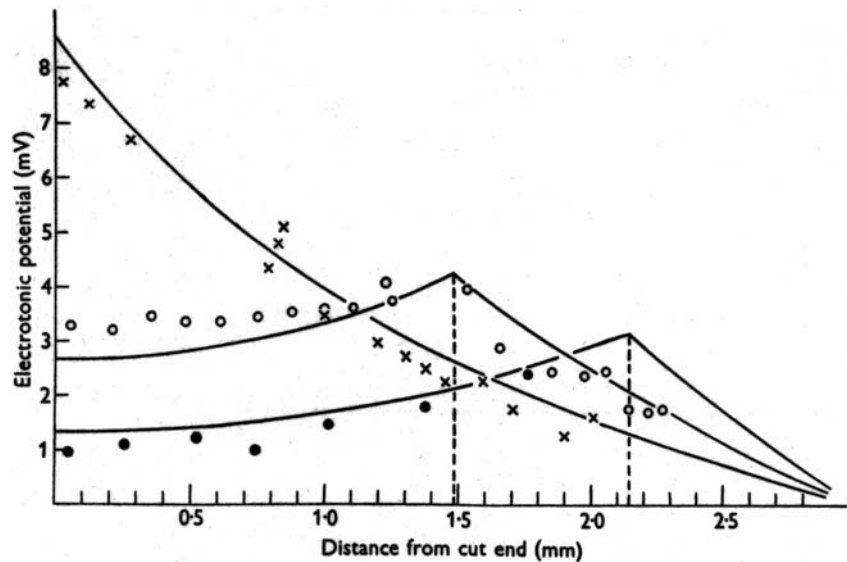


Figure 7-21: Data points show the change in membrane potential when square current steps were made in a cardiac Purkinje fiber. Voltage change was measured at various distances along the fiber (ordinate). The abscissa is distance, mm, from the cut end. Current was injected at three points,  $x = 0.02$  mm (cross),  $x = 1.48$  mm (open circle), and  $x = 2.14$  mm (solid circle). The lines are drawn from the one-dimensional cable equation, Eq. 7-83. (From Weidmann, 1952, with permission.)

For the Purkinje fibres  $R_i$  is about 100  $\Omega/\text{cm}$ ,  $R_m$  is about 20,000  $\Omega/\text{cm}^2$ ,  $\lambda_m$  is about 2 mm,  $\tau_m$  is about 20 ms, and  $C_m$  is about 1  $\mu\text{F}/\text{cm}^2$ . It may be seen from the figure that the diminution in  $V_0$  is more than the factor of 2.0 expected from the theory; this is presumably due to the finite length of the preparation, allowing leak of current from the opposite end.

### 7-7.2. The velocity of propagation

Consider first the propagation along a nerve or muscle fiber with uniform properties along the length. This would apply to an *unmyelinated* nerve. The regenerative depolarization due to the opening of the Na channels drives the continuous propagation along a nerve or Purkinje fibre. The rate of depolarization,  $dV_m/dt$  is proportional to the current flow  $i_m$ , so when the conduction velocity,  $\Theta$  m/s, becomes constant then the second derivative of voltage with respect to position  $x$

is the second derivative of voltage with respect to time at the same  $x$  divided by the conduction velocity squared:

$$\frac{\partial^2 V_m}{\partial x^2} = \frac{1}{\Theta^2} \cdot \frac{\partial^2 V_m}{\partial t^2}, \quad (7-87)$$

which on combining with the cable equation, Eq. 7-79, gives us

$$\frac{1}{r_i \Theta^2} \cdot \frac{\partial^2 V_m}{\partial t^2} = \frac{V_m}{r_m} + c_m \cdot \frac{\partial V_m}{\partial t} \text{ or} \quad (7-88)$$

$$\frac{1}{r_i \Theta^2} \cdot \frac{\partial^2 V_m}{\partial t^2} = i_m + c_m \cdot \frac{\partial V_m}{\partial t}, \quad (7-89)$$

since the transmembrane current is  $V_m/r_m$ . Most commonly this is the Na current, but smooth muscle cells and partially depolarized cardiac cells will be driven by the relatively slow calcium inward current, resulting in a slower propagation velocity. In Purkinje fibres  $\Theta$  is about 3 m/s, due to a combination of large diameter and high conductivity Na channels, which is very high relative to cardiomyocyte-to-cardiomyocyte propagation. Smooth muscles, with poorer gap junctional connections and smaller diameters, may exhibit velocities only 1/1000 of this.

A good generality is that, internal resistances and transmembrane conductances being the same, the velocity is proportional to the square root of the diameter of the cable:

$$\theta^2 \propto \text{diameter} \quad \text{or} \quad \theta \propto \sqrt{r}. \quad (7-90)$$

The conduction velocity,  $\theta$ , is speeded up by low internal longitudinal resistance,  $R_i$ , low membrane capacitance,  $C_m$ , and high resistance across the membrane, i.e., low transmural conductance. Hunter, McNaughton and Noble (1975) derived a model function accounting for the delayed activation due to the  $m^3$  for the Na conductance  $g_{Na}$  and the rate,  $k$ , at which  $g_{Na}$  was activated:

$$\theta \propto \left(\frac{d}{R_i}\right)^{1/2} \cdot (k g_{Na})^{1/8} \cdot C_m^{-5/8}. \quad (7-91)$$

The delay in activation increases  $\theta$ , and a high conduction velocity prevents  $g_{Na}$  from activating fully at the wave front and explaining the power of 1/8 on this term. The topic of conduction velocity is covered in detail by Jack, Noble and Tsien (1975) in their section on nonlinear cable theory.

A myelinated nerve has a higher conduction velocity, for several reasons. The first is the insulating and capacitative effect of the myelin sheath. The sheath consists of multiple layers of lipid bilayer membrane wrapped around the original nerve fiber. This is quite a thick layer, and is commonly found near the optimal thickness of about 40% of the diameter of the nerve fiber,

leaving 60% for the cytoplasm. The high membrane resistance lengthens the space constant (Eq. 7-80), and greatly increases  $\theta$ . The propagation is maintained by activation of the regenerative Na current at periodically positioned circumferential bare patches, the Nodes of Ranvier, where there is no insulation and a plethora of Na channel proteins. The propagation proceeds therefore by activation of regenerative depolarization at the nodes combined with passive propagation due to a very long space constant, reaching the next node with high enough voltage to trigger its Na channels to open. This jumping from node to node is “saltatory conduction”.

## 7-8. Maintaining ionic balance: Pumps and exchangers

The major roles of the pumps are to maintain the intracellular concentration of  $\text{Ca}^{2+}$  at a low level and that of intracellular  $\text{K}^+$  at a high level. The level of intracellular Na is in most cells also kept low, at about 10% of the extracellular level, for the Na gradient serves as the driving force for the extrusion of  $\text{Ca}^{2+}$  and of  $\text{H}^+$ . This is a complex situation since there are continuous leaks and periodic time and voltage dependent current fluxes which are to be balanced by these recovery processes, which must respond to the fluctuating demands placed upon them with varying rates of excitation, varied ionic gradients, and variable supplies of energy to drive them.

There are three major ATP-driven pumps, the NaK ATPase, the plasmalemmal CaATPase, and the CaATPase of the sarcoplasmic reticulum (the SERCA pump). The NaK ATPase extrudes 3  $\text{Na}^+$  in exchange for 2  $\text{K}^+$ , and is thus electrogenic, and uses 1 ATP (approximately) for each stoichiometric exchange. The CaATPases are less well defined, and may use  $\text{Mg}^{2+}$ ,  $\text{K}^+$  or  $\text{H}^+$  as counterions. All of these pumps are reversible in the full sense of the term: at low intracellular ATP levels they can be run backward by the concentration gradients to produce ATP from ADP and  $P_i$ .

On the cell membrane there is an additional  $\text{Ca}^{2+}$  extrusion process, the NaCa exchanger, NaCaX. It is electrogenic and bi-directional, exchanging three  $\text{Na}^+$  for one  $\text{Ca}^{2+}$ , depolarizing the cell a little when the cell is near the resting potential. In a minimal system, only two of the three plasmalemmal exchange mechanisms are needed: if the Na-K exchange is handled by the NaK ATPase, then one might get by with only the NaCaX or the CaATPase. There are species of sheep without the NaK ATPase on their RBC membranes (Tosteson and Hoffman, 1960); the cells are equipped with the NaCaX and the CaATPase, but function with much lower  $[\text{K}^+]_i$  than other RBC. This would not work for excitable cells since the resting membrane potential is too near zero to inactivate the fast inward Na channel, which requires depolarization to below  $-60$  mV.

Defining model equations for the pumps and exchangers requires extensive experimental data on the mechanisms and kinetics. The pumps have been the subject of ingenious experiments to uncover the sequence of events involved in ATP binding, the changes in conformational state and the release of  $P_i$ , the translocation of the carried ion and so on. This complex topic will be covered in Chapter 8 on Transporters.

## 7-9. Volume changes with ionic fluxes

[Post-Jolly expression for cell water balance (missing section).]

**[In this section describe the Post-Jolly approach, show its inadequacy for practical implementation. Then derive a stronger approach to providing osmotic balance in the presence of a Donnan, and account for pump fluxes. Provide a model and a program giving**

**a true Steady State. This actually is a new research, but is needed for rounding out the ideas in this book.**

**The Endresen and Hall ionic cell (Endresen et al., 2000) illustrates the balancing act.**

## 7-10. Summary

[No material. -ed.]

## 7-11. Further reading

**[To be revised.]** The classic works on the research and understanding of electrophysiology and the nerve action potential are reviewed and evaluated in careful detail in Jack, Noble and Tsien (1975) and Hille (2001). Less detailed and less demanding texts are those of RB Stein (1980), and WD Stein (1990), both of which provide excellent perspectives without as much mathematics. For the mathematically inclined the book by Keener and Sneyd (1998) covers this topic exceedingly well and presents phase plane analysis of the action potential models.

Recent work in cardiac electrophysiology is presented in journal issues put together from symposia on the topic, ???

For this section see the website <http://www.physiome.org>, in particular the ModelDB/Cardiovascular/Electrophysiology/index.htm page.

## 7-12. Problems

1. If  $E_R$  is  $-90$  mV in a cardiac cell, and if all cation conductances except that for  $K^+$  are zero, and  $[K^+]_o$  is 5 mM, what is the intracellular concentration  $[K^+]_i$ ? Use the Nernst equation.
2. Show that RC has the units of time. Use the Terminology to provide conversion factors.
3. List the time- and voltage-dependent variables in the Hodgkin-Huxley nerve action potential model. Which of these are most important in determining the following: (a) a threshold for regenerative depolarization; (b) the voltage achieved at the peak of the action potential; (c) the rapid repolarization phase; (d) a phase of unexcitability following repolarization; (e) accommodation to a slowly rising stimulus, seen as an increase in the threshold for regenerative depolarization.
4. Given the Nernst expression for  $E_K$  and a version of the Goldman equation for the resting membrane potential that includes Na and K permeabilities, and an augmentation by the NaKATPase of an additional depolarization by 8 mV, and given that  $P_{Na}/P_K = r$ , find the point of intersection between the Goldman and the Nernst relationships as  $[K^+]_o$  is changed while keeping  $[K^+]_i$  constant at 150 mM. Give values of  $E_m$  for  $r = 0.01$ .
5. The H-H variable  $m$  changes with gate opening rate  $\alpha$  and closing rate  $\beta$ , such that the fraction of open  $m$  gates is determined through a differential equation  $dm/dt = \alpha - (\alpha + \beta)m$ . Show that  $m_\infty = \alpha/(\alpha + \beta)$ , and  $\tau_\infty = 1/(\alpha + \beta)$ .
6. Develop a method to calculate the maximum rate of rise of the action potential for the H-H model of the squid giant axon. How would you do this experimentally using a circuit?
7. Describe the effects on the space constant of a branch in the cable into two. What are the effects of enlarging or shrinking cross-sectional areas, while assuming that the densities of channels per unit surface area remains constant.
8. Estimate conduction velocities for nerves of diameter 20, 50 and 200  $\mu\text{m}$ . Take values for suitable constants from this chapter.

9. Show how Eq. 7-83 is a solution to the differential equation of the type

$$\frac{\partial^2 V}{\partial x^2} + V = i(x - \varepsilon), \quad (7-92)$$

where  $\varepsilon$  is a position along the cable.

## 7-13. References

- [7503.](#) Akaike N. Development of pump electrogenesis in hypokalaemic rat muscle. *Pflügers Arch* 379: 215-218, 1979.
- [10080.](#) Bassingthwaighte JB and Reuter H. Calcium movements and excitation-contraction coupling in cardiac cells. *Electrical Phenomena in the Heart*, edited by DeMello WC. New York: Academic Press, Inc., 1972, p. 353-395.
- [10134.](#) Bassingthwaighte JB, Fry CH, and McGuigan JAS. Relationship between internal calcium and outward current in mammalian ventricular muscle; A mechanism for the control of the action potential duration?. *J Physiol* 262: 15-37, 1976.
- [10400.](#) Bassingthwaighte JB, Liebovitch LS, and West BJ. *Fractal Physiology* New York, London: Oxford University Press, 1994, 364 pp.
- [2450.](#) Beeler GW Jr and Reuter H. Membrane calcium current in ventricular myocardial fibres. *J Physiol* 207: 191-209, 1970.
- [683.](#) Beeler GW Jr and Reuter H. Reconstruction of the action potential of ventricular myocardial fibres. *J Physiol (Lond)* 268: 177-210, 1977.
- [5751.](#) Beran J. *Statistics for long-memory processes* New York: Chapman & Hall, 1994, 315 pp.
- [7530.](#) Cole KS and Curtis HJ. Electric impedance of the squid giant axon during activity. *J Gen Physiol* 22: 649-670, 1939.
- [2357.](#) Cole KS and Moore JW. Potassium ion current in the squid giant axon: dynamic characteristic. *Biophys J* 1: 1-14, 1960.
- [7531.](#) Curtis H and Cole K. Membrane action potentials from the squid giant axon. *J Cell Comp Physiol* 15: 147-152, 1940.
- [7532.](#) Curtis H and Cole K. Membrane resting and action potentials from the squid giant axon. *J Cell Comp Physiol* 19: 135-144, 1942.
- [7701.](#) Endresen LP, Hall K, Hoyer JS, and Myrheim J. A theory for the membrane potential of living cells. *Eur Biophys J* 29: 90-103, 2000.
- [5274.](#) Fitzhugh R. Impulses and physiological states in theoretical models of nerve membrane. *Biophys J* 1: 445-466, 1961.
- [7508.](#) Glaser R. *Biophysics* Berlin/Heidelberg/New York: Springer, 2000, 361 pp.
- [3749.](#) Goldman DE. Potential, impedance, and rectification in membranes. *J Gen Physiol* 27: 37-60, 1943.
- [7845.](#) Goudet C, Benitah JP, Milat ML, Sentenac H, and Thibaud JB. Cluster organization and pore structure of ion channels formed by beticolin 3, a nonpeptidic fungal toxin. *Biophys J* 77: 3052-3059, 1999.
- [6795.](#) Greenstein JL, Wu R, Po S, Tomaselli GF, and Winslow RL. Role of the calcium-independent transient outward current  $I_{to1}$  in shaping action potential morphology and duration. *Circ Res* 87: 1026-1033, 2000.

- [5107](#). Hille B. *Ionic Channels of Excitable Membranes* Sunderland, Mass.: Sinauer Associates, 1984, 426 pp.
- [7133](#). Hille B. *Ion Channels of Excitable Membranes, Third Edition* Sunderland, Massachusetts: Sinauer Associates, 2001, 814 pp.
- [3743](#). Hodgkin AL and Katz B. The effect of sodium ions on the electrical activity of the giant axon of the squid. *J Physiol* 108: 37-77, 1949.
- [7526](#). Hodgkin AL, Huxley AF, and Katz B. Measurement of current-voltage relations in the membrane of the giant axon of *Loligo*. *J Physiol* 116: 424-448, 1952a.
- [7527](#). Hodgkin AL and Huxley AF. Currents carried by sodium and potassium ions through the membrane of the giant axon of *Loligo*. *J Physiol* 116: 449-472, 1952b.
- [7528](#). Hodgkin AL and Huxley AF. The components of membrane conductance in the giant axon of *Loligo*. *J Physiol* 116: 473-496, 1952c.
- [7529](#). Hodgkin AL and Huxley AF. The dual effect of membrane potential on sodium conductance in the giant axon of *Loligo*. *J Physiol* 116: 497-506, 1952d.
- [700](#). Hodgkin AL and Huxley AF. A quantitative description of membrane current and its application to conduction and excitation in nerve. *J Physiol* 117: 500-544, 1952e.
- [7846](#). Hunter PJ, McNaughton PA, and Noble D. Analytical models of propagation in excitable cells. *Prog Biophys Molec Biol* 30: 99-114, 1975.
- [7504](#). Jack JJB, Noble D, and Tsien RW. *Electric Current Flow in Excitable Cells* Oxford, England: Clarendon Press, 1975, 502 pp.
- [6440](#). Jafri MS, Rice JJ, and Winslow RL. Cardiac  $\text{Ca}^{2+}$  dynamics: The roles of ryanodine receptor adaptation and sarcoplasmic reticulum load. *Biophys J* 74: 1149-1168, 1998.
- [6661](#). Keener J and Sneyd J. *Mathematical Physiology* New York, NY: Springer-Verlag, 1998, 766 pp.
- [6851](#). Kohl P, Hunter P, and Noble D. Stretch-induced changes in heart rate and rhythm: clinical observations, experiments and mathematical models. *Prog Biophys Mol Biol* 71: 91-138, 1999.
- [7466](#). Lauger P. Kinetic basis of voltage dependence of the Na,K-pump. *Soc Gen Physiol Ser* 46: 303-315, 1991.
- [3036](#). Liebovitch LS. Testing fractal and Markov models of ion channel kinetics. *Biophys J* 55: 373-377, 1989.
- [5062](#). Luo C and Rudy Y. A model of the ventricular cardiac action potential: Depolarization, repolarization, and their interaction. *Circ Res* 68: 1501-1526, 1991.
- [6337](#). Luo C-H and Rudy Y. A dynamic model of the cardiac ventricular action potential I. Simulations of ionic currents and concentration changes. *Circ Res* 74: 1071-1096, 1994.
- [5565](#). Luo C-H and Rudy Y. A dynamic model of the cardiac ventricular action potential: II: Afterdepolarizations, triggered activity, and potentiation. *Circ Res* 74: 1097-1113, 1994.
- [7127](#). Michailova A and McCulloch A. Model study of ATP and ADP buffering, transport of  $\text{Ca}^{2+}$  and  $\text{Mg}^{2+}$ , and regulation of ion pumps in ventricular myocyte. *Biophys J* 81: 614-629, 2001.
- [7480](#). Mullins LJ and Noda K. The influence of sodium-free solutions on the membrane potential of frog sartorius muscle. *J Gen Physiol* 47: 117-132, 1963.
- [5275](#). Nagumo J, Arimoto S, and Yoshizawa S. An active pulse transmission line simulating nerve axon. *Proc IRE* 50: 2061-2070, 1962.
- [7534](#). Noble D. A modification of the Hodgkin-Huxley equations applicable to Purkinje fibre action and pace-make potentials. *J Physiol* 160: 317-352, 1962.

- [6849](#). Noble D, Varghese A, Kohl P, and Noble P. Improved guinea pig ventricular cell model incorporating a diadic space,  $I_{Kr}$  and  $I_{Ks}$ , and length- and tension-dependent processes. *Canad J Cardiol* 14: 123-134, 1998.
- [7539](#). Rall W. Core conductor theory and cable properties of neurons. *Handbook of Physiology (Section 1): The Nervous System I. Cellular Biology of Neurons*, edited by Kandel ER. Baltimore, MD: American Physiological Society, 1977, p. 39-97.
- [7198](#). Sachs F. Modeling mechanical-electrical transduction in the heart. *Cell Mechanics and Cellular Engineering*, edited by Mow C, Guilak F, Tran-Son-Tay R, and Hochmuth RM. New York: Springer, 1994, p. 308-328.
- [5122](#). Sakmann B and Neher E (Editors). *Single-Channel Recording* New York: Plenum Press, 1983, 503 pp.
- [7535](#). Sakmann B and Neher E (Editors). *Single-channel Recording. Second Edition* New York: Plenum, 1995, 700 pp.
- [7538](#). Sakmann BF, Spindler AJ, Bryant SM, Linz KW, and Noble D. Distribution of a persistent sodium current across the ventricular wall in guinea pigs. *Circ Res* 87: 964-965, 2000.
- [711](#). Sperelakis N. Origin of the cardiac resting potential. Appendix: Physical principles, derivations, and applications. *Handbook of Physiology, Sec. 2, The Cardiovascular System. Vol. 1*, edited by Berne RM, Sperelakis N, and Geiger SR. Baltimore: Waverly Press, Inc., 1979, p. 187-267.
- [7505](#). Stein RB. *Nerve and Muscle: Membranes, Cells, and Systems* New York, New York: Plenum Press, 1980, 265 pp.
- [4733](#). Stein WD. *Channels, Carriers and Pumps: An Introduction to Membrane Transport* San Diego, CA: Academic Press, 1990, 326 pp.
- [7501](#). Tamai T and Kagiya S. Studies of cat heart muscle during recovery after prolonged hypothermia. *Circ Res* 1968: 423-433, 22.
- [1453](#). Tosteson DC and Hoffman JF. Regulation of cell volume by active cation transport in high and low potassium sheep red cells. *J Gen Physiol* 44: 169-194, 1960.
- [3755](#). Weidmann S. The electrical constants of Purkinje fibres. *J Physiol* 118: 348-360, 1952.
- [7533](#). Weidmann S. Shortening of the cardiac action potential due to a brief injection of KCl following the onset of activity. *J Physiol* 132: 156-163, 1956.
- [6646](#). Winslow RL, Rice J, Jafri S, Marbán E, and O'Rourke B. Mechanisms of altered excitation-contraction coupling in canine tachycardia-induced heart failure, II: Model studies. *Circ Res* 84: 571-586, 1999.
- [7844](#). Zhang P, Fyfe GK, Grichtchenko II, and Canessa CM. Inhibition of alphabeta epithelial sodium channels by external protons indicates that the second hydrophobic domain contains structural elements for closing the pore. *Biophys J* 77: 3043-3051, 1999.

#### 7-13.1. [References not cited in current text](#)

6698. Winslow RL, Scollan DF, Holmes A, Yung CK, Zhang J, and Jafri MS. Electrophysical modeling of cardiac ventricular function: From cell to organ. *Ann Rev Biomed Eng* 2: 119-155, 2000.
7483. Winslow RL, Greenstein JL, Tomaselli GF, and O'Rourke B. Computational models of the failing myocyte: relating altered gene expression to cellular function. *Phil Trans R Soc Lond A* 359: 1187-1200, 2001.

7183. Mazhari R, Greenstein JL, Winslow RL, Marbán E, and Nuss HB. Molecular interactions between two long-QT syndrome gene products, HERG and KCNE2, rationalized by in vitro and in silico analysis. *Circ Res* 89: 33-38, 2001.